

Quantifying the sensitivity of L-Band SAR to a decade of vegetation structure changes in savannas

Konrad Wessels ^{a,*}, Xiaoxuan Li ^a, Alexandre Bouvet ^b, Renaud Mathieu ^c, Russell Main ^d, Laven Naidoo ^e, Barend Erasmus ^f, Gregory P. Asner ^g

^a Department of Geography and GeoInformation Science, George Mason University, Fairfax, VA, USA

^b Centre d'Etudes Spatiales de la Biosphère (CESBIO), Université de Toulouse, CNES/CNRS/INRAE/IRD/UPS, Toulouse, France

^c International Rice Research Institute, South Asia Research Center, Varanasi, India

^d Council for Scientific and Industrial Research (CSIR), Pretoria, South Africa

^e Gauteng City-Region Observatory (GCRO), Johannesburg, South Africa

^f Faculty of Natural and Agricultural Sciences, University of Pretoria, South Africa

^g Center for Global Discovery and Conservation Science, Arizona State University, Tempe, USA

ARTICLE INFO

Edited by Jing M. Chen

Keywords:

SAR

Savannas

L-Band

LiDAR

Vegetation structure

ALOS PALSAR

South Africa

ABSTRACT

Global savannas are the third largest carbon sink with large human populations being highly dependent on their ecosystem services. However, savannas are changing rapidly due to climate change, fire, animal management, and intense fuelwood harvesting. In southern Africa, large trees (>5 m in height) are under threat while shrub cover (<3 m) is increasing. The collection of multi-date airborne LiDAR (ALS) data, initiated over a decade ago in the Lowveld of South Africa, provided a rare opportunity to quantify the ability of L-band SAR to track changes in savanna vegetation structure and this study is the first to do so, to our knowledge. The objective was to test the ability of ALOS PALSAR 1&2, dual-pol (HH, HV) data to quantify woody cover and volume change in savannas over 2-, 8- and 10-year periods through comparison to ALS. For each epoch (2008, 2010, 2018), multiple PALSAR images were processed to Gamma 0 (γ^0) at 15 m resolution with multi-temporal speckle filtering. ALS data were processed to fractional canopy cover and volume, and then compared to 5×5 aggregated (75 m) SAR mean γ^0 . The ALS cover change (ΔC_{ALS}) and volume change between pairs of years were highly correlated, with ($R^2 > 0.8$), thus results for cover change applied equally to volume change. Cover change was predicted using (i) direct backscatter change or (ii) the difference between annual cover map product derived using the Bayesian Water Cloud Model (BPCM) and logarithmic models. The linear relationship between $\Delta\gamma^0$ and ΔC_{ALS} varied between year pairs but reached a maximum R^2 of 0.7 for 2018–2010 and a moderate R^2 of 0.4 for 2018–2008. Overall, 1 dB $\Delta\gamma^0$ corresponded to approximately 0.1 cover change. The three cover change models had very similar uncertainties with mean RMSE = 0.15, which is 13% of the observed cover change range (-0.6 to $+0.6$). The direct backscatter change approach had less underestimation of positive and negative cover change. The L-band backscatter had a higher sensitivity than suggested by previous studies, as it was able to reliably distinguish cover change at 0.25 increments. The SAR-derived cover change maps detected the loss of stands of big trees, and widespread increases in cover of 0.35–0.65 in communal rangelands due to shrub encroachment. In contrast, the maps suggest that cover generally decreased in conservation areas, forming distinct fence-line effects, potentially caused by significant increases in elephant numbers and frequent, intense wildfires in reserves.

1. Introduction

Savanna ecosystems consist of a spatio-temporally variable mosaic of continuous herbaceous and non-continuous woody vegetation layers and experience alternating wet and dry seasons (Bond, 2008; Scholes

and Archer, 1997b; Scholes and Walker, 1993). Although the carbon density of savannas is generally low, savannas are the third highest carbon stock after tropical and temperate forests (Grace et al., 2006; Santoro and Cartus, 2018; Saugier et al., 2001). In Africa 52% of the total above-ground carbon is stored in savannas (Bouvet et al., 2018).

* Corresponding author.

E-mail address: kwessel4@gmu.edu (K. Wessels).

Some 252 million people globally are estimated to be living in forests and savannas that have daily incomes of less than USD 1.25, with African rural communities making up 63% of that number (FAO, 2020). More than half of Africa's population lives in savannas and their livelihoods are dependent on essential ecosystem services through grazing for domestic livestock, timber and non-timber products, fuelwood extraction and wildlife-based tourism (Chidumayo and Gumbo, 2010; Scholes and Archer, 1997a; Twine et al., 2003; Twine and Holdo, 2016; Wessels et al., 2013).

The dynamic ratio of herbaceous versus woody components and its structure is determined by a combination of local factors, including, availability of water, soil properties, fire regimes, herbivory and anthropogenic disturbances (e.g. land use change, tree harvesting, livestock grazing) (Bond, 2008; Sankaran et al., 2005, 2008; Staver et al., 2011; Stevens et al., 2016), as well as global factors including, CO₂ fertilization and climate change (Bond and Midgley, 2012; Ratnam et al., 2016; Southworth et al., 2016). Changes in woody vegetation include both losses and gains; the loss due to drought, logging, high elephant densities (Asner et al., 2016; Davies et al., 2018; Dean et al., 1999; Levick et al., 2009; Mograbi et al., 2015, 2017; Smit and Prins, 2015; Wessels et al., 2011) and gains due to fire suppression, livestock overgrazing, and long-term interactions between fire and rainfall episodes (Joubert et al., 2013; O'Connor et al., 2014). Spatial information on changes in vegetation structure is essential to making informed management decisions related to livestock ranching, wildlife and biodiversity conservation, debushing of shrub encroachment and fire management (Smit et al., 2010, 2016; Smit and Prins, 2015; Venter et al., 2018). In addition, international initiatives, such as REDD+ (Reduced Emissions from Deforestation and Degradation), which seek to incentivize the conservation of ecosystem services and biodiversity through sustainable forest management practices, also require accurate quantification of the woody vegetation structure (specifically above ground biomass) (Mitchard et al., 2013; Mitchell et al., 2017).

Three-dimensional woody vegetation structure is defined as the vertical configuration of aboveground vegetation and its horizontal, leaf to landscape scale variations (Bergen et al., 2009; Brokaw and Lent, 1999). The horizontal variation in vegetation can be described by the woody canopy cover, i.e. the vertical projection of canopies on a horizontal plane (Jennings et al., 1999). Woody cover is a simple, and widely used, two-dimensional structural indicator that can provide landscape level information regarding spatial extent and heterogeneity of woody vegetation, habitat fragmentation, and patchiness (Turner and Gardner, 2001). Woody cover change derived from remote sensing satellite data and historical vs. recent aerial photographs have been widely used to investigate ecological trends and human impacts on woody vegetation structure (Anchang et al., 2020; Bastin et al., 2017; Mitchard et al., 2013; Skowno et al., 2017; Stevens et al., 2016; Tian et al., 2017; Venter et al., 2018; Wagenseil and Samimi, 2007; Wessels et al., 2019). By adding vertical structure information, such as canopy height, to woody cover, a simple three-dimensional expression of canopy volume can be calculated as a proxy for biomass (Camarretta et al., 2019; Colgan et al., 2012; Thorne et al., 2002). This study investigated both woody cover and volume changes in vegetation structure.

Airborne LiDAR scanners (ALS) provide detailed and accurate data on three-dimensional woody vegetation structure (Camarretta et al., 2019) and have been used to conduct research into some of the foremost ecological topics in savannas (Asner et al., 2016; Davies et al., 2018; Dean et al., 1999; Fisher et al., 2012, 2015; Levick et al., 2009; Mograbi et al., 2015, 2017; Smit et al., 2016; Smit and Prins, 2015; Wessels et al., 2011, 2013). However, the ALS data are expensive, limited in spatial coverage and infrequently repeated for the same area, especially in developing countries, which limits long-term monitoring at regional scales. Space-borne synthetic aperture radar (SAR) has therefore become an attractive option due to its wide coverage, relative affordability, and multi-temporal acquisition ability. Radar backscatter at a given wavelength and polarization is a function of the target's (i) structural or

geometric properties and (ii) dielectric properties. Structural properties of vegetation canopies are influenced by the size and distribution of scatterers (main stem, branches, and foliage) relative to wavelength, orientation of scatterers, and number of scattering elements (Bergen et al., 2009; Bergen and Dobson, 1999). Dielectric properties are a function of volumetric water content, the phase of water (liquid or frozen), and the specific dry density of the scatterers. Depending on the microwave wavelength, polarization and incidence angle, the microwaves penetrate the canopy, interact with canopy scatterers, and subsequently create a volume scattering response (Clark et al., 2011; Dobson et al., 1992). Volumetric response also changes the polarization or orientation of the microwave's electric field and as a result, the cross-polarised signals (VH, HV) generally show higher volumetric responses than co-polarised signals (VV, HH). This volume scattering response is what lends SAR imagery so favourably to regional scale mapping of vegetation structure, particularly forest extent (Rosenqvist et al., 2003) and the detection of deforestation and degradation (Ryan et al., 2012; Woodhouse et al., 2012). Volume scattering responses are at a maximum when the size of the canopy scatterers is in the same order as the microwave wavelengths (Dobson et al., 1992; Le Toan et al., 2004; Woodhouse, 2006). Shorter wavelengths (i.e. X- & C-band) generally interact with the smaller components of the top of canopies (i.e. twigs, leaves, and small branches), whereas the longer wavelengths (i.e. L- & P-band) penetrate further into the canopy and interact with larger branches and trunks (Woodhouse, 2006). Because of its capability to penetrate into vegetation canopies, SAR measurements are more directly related to forest volume and biomass, particularly at long radar wavelengths such as L-band (~23 cm) and P-band (~70 cm wavelength) (Cartus et al., 2014). However, backscatter is also influenced by other surface properties, such as highly variable vegetation and soil moisture, forest types, surface roughness (rocky outcrops) and topography, especially in low biomass savannas where microwaves easily reach the ground and where there is a low vegetation signal-to-noise ratio (Lucas et al., 2010).

Recent studies in savannas have demonstrated that L-band SAR backscatter has a much stronger relationship with woody vegetation cover and biomass than shorter wavelength, X-band or C-band SAR (Main et al., 2016; Mathieu et al., 2013; Urbazaev et al., 2015), since the backscatter of longer wavelengths is largely due to interactions with branches and stems rather than leaves which are highly variable through time (Mitchard, 2009; Lucas et al., 2010). While a wide range of algorithms have been developed for estimating structure variables of forests, these are less applicable to savannas where open canopies and greater variability in the location, size, number and density of woody components (e.g., stems) leads to a greater diversity of microwave interactions with the ground surfaces and vegetation (Lucas et al., 2010; Smith et al., 2019). Although L-band backscatter reaches saturation at 70–120 Mg/ha forest biomass, which limits its application in very high biomass tropical forests (Bouvet et al., 2018; Joshi et al., 2017; Lucas et al., 2010; Yu and Saatchi, 2016), it has the appropriate sensitivity range for savannas that typically vary from 10–90 Mg/ha (Colgan et al., 2012; Naidoo et al., 2015; Odipo et al., 2016). A number of studies have demonstrated a useful relationship between L-band SAR and savanna biomass in Australia (Lucas et al., 2006; Lucas et al., 2010), Brazilian cerrado (da Bispo et al., 2020; Zimbres et al., 2021), Africa, e.g., Uganda, Cameroon, Mozambique (Carreiras et al., 2013; Mermoz et al., 2014; Mitchard, 2009), Namibia (Wingate et al., 2018), and specifically, the current study area in the Lowveld of South Africa (Naidoo et al., 2015; Odipo et al., 2016). Recently, Bouvet et al. (2018) used a Bayesian inversion of the Water Cloud Model to map above-ground biomass for the African continent using 2010 ALOS PALSAR mosaics and ground based AGB estimates, with limited ALS-based validation yielding encouraging accuracies of $R^2 = 0.78$, RMSE = 6–30 Mg/ha, and relative RMSE of 30–80%. However, while the baseline relationship between L-band SAR backscatter and biomass has been established in savannas, the use of SAR to quantify woody structure change has received less

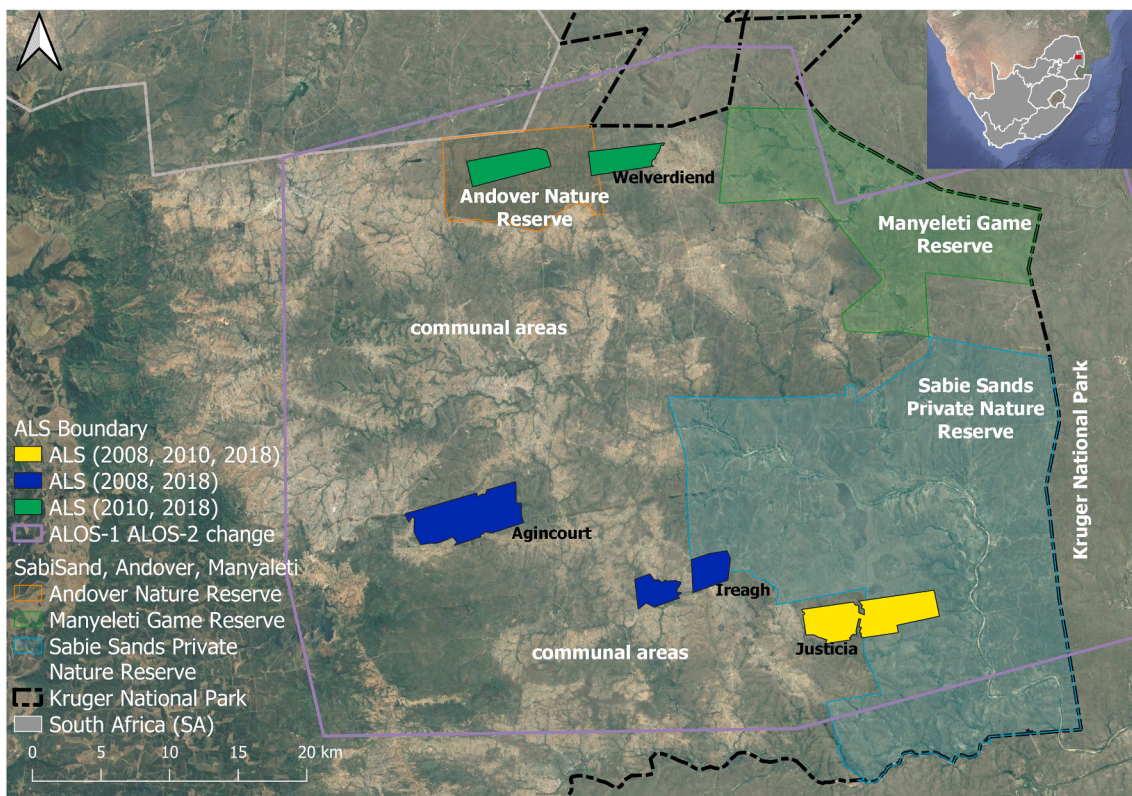


Fig. 1. Study area in the Lowveld of South Africa including Kruger National Park, other reserves and communal areas. The location of airborne LiDAR (ALS) data of different combinations of years are indicated along with the overlapping ALOS and ALOS-2 PALSAR change analysis area.

attention.

While there have been several studies on the detection of deforestation in high biomass forests (Mermoz and Le Toan, 2016; Santoro et al., 2012; Urbazaev et al., 2018), there has been a limited number of studies to demonstrate the ability of L-band SAR to detect and quantify structural changes in low-biomass savannas. Mitchard et al. (2011) was able to detect deforestation and woody encroachment along forest-savanna ecotone of central Cameroon by comparing Advanced Land Observing Satellite (ALOS) Phased Arrayed L-band Synthetic Aperture Radar (PALSAR) data with L-band JERS-1 data acquired 11 years before. Ryan et al., 2012 detected land cover change and quantified the carbon stock losses of 11–33 MgC/ha in Mozambique woodlands using ALOS PALSAR data over a three-year period. Mitchard et al., 2013 detected increases in woodland carbon of 1.1 MgC/ha/year and decreases of 3 MgC/ha/year in Mozambique with ALOS PALSAR, but highlighted the need for more rigorous quantification of uncertainty. McNicol et al., 2018 estimated changes in woodland carbon across large parts of southern Africa with ALOS PALSAR annual mosaics. They found that deforestation was 3–6 times higher than previously estimated with Landsat data (Hansen et al., 2013) and widespread degradation (defined as losses of >20% of above ground carbon). Odipo et al., 2016 suggested that changes in biomass of >5 Mg/ha could be detected by ALOS PALSAR data and models based on terrestrial LiDAR scanner training data within the Lowveld of South Africa, and encouraged future studies to fully quantify this change detection accuracy with ALS data. Wessels et al., 2019 recently demonstrated the ability of annual mosaics of ALOS PALSAR data (Shimada et al., 2014) to accurately map woody cover and detect cover changes in Namibian savannas with a fractional cover change uncertainty of RSME = 0.18, derived from the RMSE's of the annual cover products. While the cover change maps captured patterns of debushing and apparent shrub regrowth (Wessels et al., 2019), the study lacked repeat ALS data to validate the accuracy of the detected woody cover change. In fact, there is a severe lack of studies with multi-

year repeat ALS data with which to develop models and validate SAR-based change products (Cartus et al., 2018). While the detection of abrupt change due to large clear-cuts in savanna woodland may be detected with SAR, there is very little knowledge of the sensitivity of the microwave signal to gradual change such as increases in shrub density (Buitenwerf et al., 2012; Mograbi et al., 2015; O'Connor et al., 2014; Skowno et al., 2017; Stevens et al., 2017; Venter et al., 2018) or the loss of small stands of trees due to multiple causes, such as elephant damage or wildfire (Asner et al., 2016; de Boer et al., 2015; Mograbi et al., 2017; Shannon et al., 2008, 2011). The current study provided a rare opportunity to investigate the sensitivity of L-band SAR to woody cover and volume changes using repeat ALS in the Lowveld of South Africa, spanning a decade of change.

The objective of this study was to assess the ability of ALOS PALSAR 1&2, dual-pol data to quantify woody cover and volume change in savannas over two-, eight- and ten-year periods through comparison to repeat ALS data. This was accomplished by (i) testing the correlations between HH and HV backscatter with ALS-derived cover and volume for individual years, (ii) inverting the models (linear, logarithmic and Bayesian inversion of Water Cloud Model, BWCM) to produce annual maps of cover and volume from SAR data and analyse the distribution of bias, (iii) analysing the change of backscatter in relation to changes of ALS cover and volume between pair of years, (iv) predicting cover change using direct backscatter change or annual cover map product differences (BWCM and logarithmic models) and (v) comparing these SAR-derived change maps to ALS cover change to interpret local and regional spatial patterns.

2. Study area

The study area is situated within the Lowveld region of the Mpumalanga Province of South Africa (Fig. 1). The study area spans a unique land use gradient, from Kruger National Park in the east, private and

provincial game reserves in the middle, to communal rangelands and rural villages in the west. Each of these land uses impact the natural savanna vegetation differently through various drivers. In conservation areas the drivers are elephants, controlled wildfire, watering points, bush thinning, while in communal areas they are selective logging, livestock grazing and fuelwood removal (Wessels et al., 2011, 2013). The national park focuses on large-scale biodiversity conservation with minimal anthropogenic influence while the private reserves manage their land to optimize eco-tourism and game viewing, which includes mechanical bush thinning. Parts of the communal areas are densely populated with >300 people /km², concentrated in rural villages including Ireagh, Justicia, Agincourt, Xanthia and Welverdiend (Coetzer-Hanack et al., 2016; Pollard et al., 2003; Twine and Holdo, 2016). The provincial game reserve of Andover, adjacent to the village of Welverdiend has experienced extensive logging inside the reserve in recent years as its status as a conservation area has been repeatedly challenged by neighboring locals.

The study area is characterized by a short, dry winter and a wet summer with mean annual rainfall ranging from 580 mm/yr to 800 mm/yr across an east-to-west increasing rainfall gradient and moderate mean annual temperatures ranging from 21 to 25 °C. High population densities coupled with historic injustices and dwindling employment, resulted in the human populace to rely heavily on the harvesting of natural resources within the communal areas (Coetzer-Hanack et al., 2016). Such activities include the harvesting of fuelwood for energy as well as the harvesting of tree bark and other products such as fruit and nuts for consumption and medicinal purposes (Shackleton, 2002; Twine and Holdo, 2016; Wessels et al., 2011). Within the protected areas, the woody vegetation structure is heavily shaped and impacted by treefall resulting from the high population density of elephants (Asner et al., 2016; de Boer et al., 2015; Mograbi et al., 2017). The woody vegetation in the region has a canopy cover ranging from 20~60%, a height range of 1.6 to 5 m and above ground biomass below 60 t/ha (Mathieu et al., 2013). The study area is classified as Tropical Dry Forest according to the FAO's Global Ecological zones (FAO, 2015) and the specific vegetation types include Clay Thornbush, Mixed Bushveld, Granite Lowveld, Sweet Lowveld Bushveld and Legogote Sour Bushveld (Mucina and Rutherford, 2006). Granite, basalt and gabbro are the dominant geological substrates in the study area. The topography of the study area is flat or gently undulating and the mean slope derived from ALS DEM is 5° (standard deviation <3°).

3. Data

3.1. ALS data

The 2008 and 2010 LiDAR data were acquired using the Carnegie Airborne Observatory (CAO) Alpha system (Asner, 2007), presently known as the Global Airborne Observatory (GAO). Both acquisitions used the same customized Optech ALTM-3100EA and instrument settings to acquire the data toward the end of the wet season, namely April. The flights occurred at 1000 m above ground level, with a 70 kHz laser pulse repetition rate, and a 50% flight line overlap, which resulted in LiDAR measurements with an average point density of 1.66 points/m².

The 2018 datasets were collected by a commercial service provider using Optech ALTM M300 and Optech Gemini sensors at 700 m above ground level with laser pulse repetition rates between 100 and 150 kHz. Acquisitions had 25% overlap between flight lines and an average point density of 8.6 points/m². The total area of ALS data collected in 2018 was 75.55 km². The acquisitions took place at the start of the dry season, namely May–June. Digital terrain models (DTM), digital surface models (DSM), and canopy height models (CHM) were generated from the ALS data at 1 m resolution, using lidR package in R (Roussel et al., 2018).

3.2. SAR data and processing

Data from the L-band satellite SAR systems ALOS PALSAR and ALOS-2 PALSAR-2 operated by the Japanese Aerospace Exploration Agency (JAXA) have been used for the 2007–2010 and 2017–2018 epochs respectively.

The two sensors have different imaging geometries and acquire data in different observation modes. Therefore, in order to compare backscatter measurements from PALSAR and PALSAR-2, specific steps were taken during data selection and processing. In addition, environmental conditions such as soil moisture or vegetation water content affect the relationships between backscatter and vegetation structural parameters. Previous studies demonstrated that the best sensitivity is observed in the dry season, when the soil moisture is consistently low and most trees have lost their leaves (Bouvet et al., 2018; Mathieu et al., 2013; Naidoo et al., 2015, 2016). Therefore, in this study, the relationships between backscatter and vegetation parameters were assessed only with dry season images.

The data availability of ALOS PALSAR was relatively sparse for the study area with approx. one acquisition per year in each orbit path, in the dry season (June to September). Five ALOS PALSAR scenes were available in Fine-Beam Dual polarization (FBD) mode (HH and HV), with an off-nadir angle equal to 34.3°, on the following dates: 6 August 2007, 23 September 2008, 11 August 2009, 14 August 2010 and 29 September 2010. The ALOS-2 PALSAR-2 data availability was less limited and 17 scenes were acquired between 23 November 2014 and 3 May 2020 in Stripmap Fine mode, Dual-polarization (HH and HV) and an off-nadir angle of 36.2°, which was the most similar configuration to that of the ALOS PALSAR images. Two images were acquired during the dry season: 2 July 2017 and 12 August 2018. The other 15 images acquired outside the dry season were used only in the multi-temporal speckle filtering step detailed below.

All the SAR data (ALOS PALSAR and ALOS-2 PALSAR-2) were ordered in Level 1.1 format (Single-Look Complex). The SAR data pre-processing was performed using the SNAP software (SNAP - ESA Sentinel Application Platform, 2022) and included:

- Calibration, to transform the digital numbers into σ^0 backscattering coefficient
- Deskewing (ALOS PALSAR only), to transform the data from a squinted geometry to a zero-Doppler geometry
- Range-Doppler terrain correction was applied to transform the data from the SAR geometry to the ground geometry, using the 1 arcsec SRTM digital elevation model (Farr and Kobrick, 2000).

The above processing steps produced georeferenced σ^0 images with a ground sampling distance of 15 m. The following additional processing was applied:

- Topographic correction was applied to transform the σ^0 to topography-corrected γ^0 using the equation given in De Grandi et al., 2011: $\gamma_{topo}^0 = \sigma^0 * \tan(\theta_{loc}) / \sin(\theta)$, where θ is the incidence angle and θ_{loc} is the local incidence angle. This step reduces the effect of topography on the backscatter and increases the comparability of the data acquired by the two different SAR sensors.
- Multi-temporal speckle filtering using (i) all the ALOS PALSAR images (2007–2010), and (ii) all the ALOS-2 PALSAR-2 images (2014–2020) was applied to reduce the speckle noise (Bruniquel and Lopes, 1997; Quegan and Yu, 2001). In the case of PALSAR-2, images acquired outside the dry seasons were used only to increase the performance of the speckle filter.
- PALSAR/PALSAR-2 cross-calibration: although the PALSAR and PALSAR-2 data are acquired with similar off-nadir angles, it was evident that in the dry season images, the average backscatter values of the PALSAR-2 were slightly higher than that of PALSAR images. This backscatter increase could be caused by either a calibration

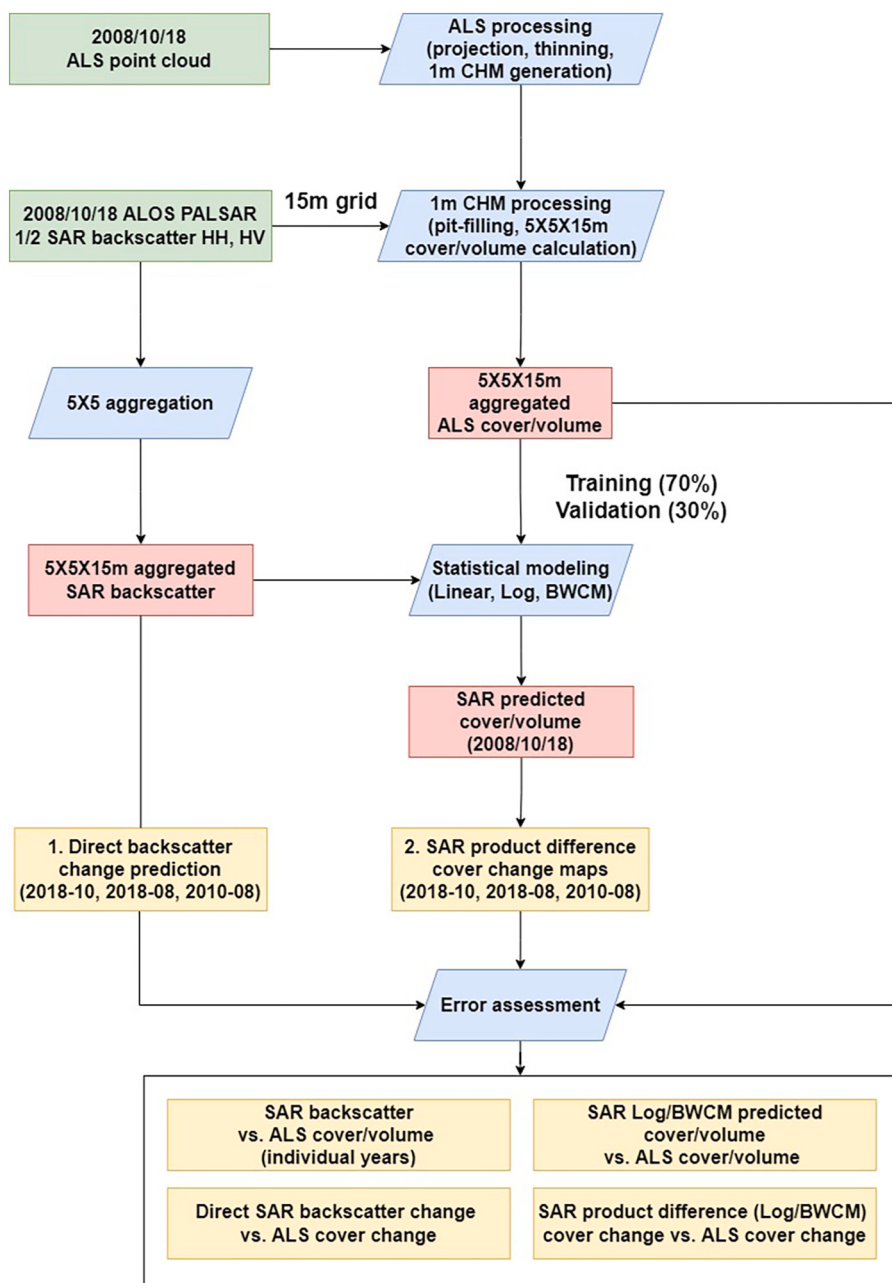


Fig. 2. Diagram of airborne LiDAR (ALS) and SAR data processing, model development, change prediction and error assessment.

discrepancy between sensors, or an actual backscatter increase, e.g., a long-term increase in the vegetation cover. After investigations of assumed stable targets (e.g., large buildings, unvegetated areas), it was found that the differences in the backscatter levels were likely due to the insufficient calibration between PALSAR and PALSAR-2, and therefore an additional small correction factor was applied, PALSAR-2 = PALSAR +0.8 dB (HH), PALSAR-2 = PALSAR +0.86 dB (HV).

4. Methods

An overview of the analysis workflow is given in Fig. 2 and detailed in subsections below. The ALS data were processed to canopy height, cover and volume within the extent of 15 m SAR pixels (Section 4.1). The SAR backscatter and ALS cover and volume metrics were compared after aggregating the 15 m resolution data to a 5 × 5, or 75 m moving window. The relationship between PALSAR backscatter and volume or

cover was investigated for individual years, using various models, i.e., linear, logarithmic and water cloud model (WCM) (Section 4.2). The next step was to invert these models to make gridded datasets for cover and volume for individual years from the SAR data. All models were run 30 times using a different, randomly selected 70% subset of data for model development and the remaining 30% for validation, while the mean results of the 30 repetitions were reported. Cover change was estimated from SAR backscatter data in two ways, (i) by directly estimating cover change from the backscatter change between two years ($\Delta\gamma^0$) (the “direct backscatter change” approach), and (ii) by calculating cover change from the difference between SAR-derived cover products of individual years (the “product difference” approach) (Section 4.3). SAR-derived cover change were compared to the ALS-derived cover change (Section 4.3). Finally maps of SAR predicted cover change were created using the model with R^2 that was closest to the mean R^2 of the 30 models and compared to ALS cover change maps (Section 5.6.4).

Table 1

Coefficient of determination (R^2) indicating the amount of variance in backscatter that is explained by the cover and volume according to linear, logarithmic and WCM.

| Year | Polarization | R^2 (linear) | R^2 (Log) | R^2 (WCM) |
|------|--------------|----------------|-------------|-------------|
| | | | | |
| 2007 | HH | 0.65 | 0.66 | 0.70 |
| 2008 | HH | 0.65 | 0.67 | 0.71 |
| 2010 | HH | 0.65 | 0.67 | 0.73 |
| 2017 | HH | 0.60 | 0.67 | 0.69 |
| 2018 | HH | 0.61 | 0.68 | 0.70 |
| Mean | HH | 0.63 | 0.67 | 0.71 |
| 2007 | HV | 0.68 | 0.69 | 0.73 |
| 2008 | HV | 0.68 | 0.69 | 0.73 |
| 2010 | HV | 0.71 | 0.71 | 0.78 |
| 2017 | HV | 0.63 | 0.73 | 0.75 |
| 2018 | HV | 0.62 | 0.72 | 0.74 |
| Mean | HV | 0.67 | 0.71 | 0.75 |

| Year | Polarization | R^2 (linear) | R^2 (Log) | R^2 (WCM) |
|------|--------------|----------------|-------------|-------------|
| | | | | |
| 2007 | HH | 0.71 | 0.68 | 0.74 |
| 2008 | HH | 0.71 | 0.69 | 0.75 |
| 2010 | HH | 0.69 | 0.69 | 0.77 |
| 2017 | HH | 0.58 | 0.62 | 0.66 |
| 2018 | HH | 0.61 | 0.64 | 0.68 |
| Mean | HH | 0.66 | 0.66 | 0.72 |
| 2007 | HV | 0.75 | 0.71 | 0.79 |
| 2008 | HV | 0.76 | 0.72 | 0.79 |
| 2010 | HV | 0.77 | 0.73 | 0.84 |
| 2017 | HV | 0.64 | 0.69 | 0.72 |
| 2018 | HV | 0.64 | 0.69 | 0.72 |
| Mean | HV | 0.71 | 0.71 | 0.77 |

4.1. Vegetation structural parameters (canopy height, cover, volume) from ALS data

Canopy height models (CHMs) were derived from the 2008, 2010, and 2018 ALS datasets. First, the 2018 LiDAR datasets were thinned to 1–1.7 points/m² in order to match the point density of the 2008 and

2010 ALS data, using the sampling function in [CloudCompare \(2019\)](#). The original 2008, 2010 and subsampled 2018 ALS point cloud were then used to generate 1 m CHMs. Next a pit-filling method ([ArcGIS Pro, 2021](#)) using focal statistics was applied to replace null values in the CHM's with the mean height of neighboring pixels. Finally, the 1 m CHMs were used to calculate ALS canopy cover and volume metrics for each corresponding 15 m SAR pixel. ALS cover fraction was calculated summing the total number of 1 m CHM pixels with heights above 1.5 m and dividing by the total number of CHM pixels in each 15 m SAR pixel. ALS volume was calculated in m³ by summing all the height values of the CHM within a coincident 15 m SAR pixel, since the x and y dimensions of the CHM was 1 m × 1 m. This calculated volume is similar to canopy projected volume and does not only include the canopy and trunk, but also the open space under the canopy ([Mathieu et al., 2013; Naidoo et al., 2015](#)). This ALS CHM-derived volume has been proven to have a strong relationship with biomass within the study area ([Colgan et al., 2012](#)).

4.2. Estimation of cover and volume from SAR backscatter for individual years

The SAR backscatter and ALS cover and volume metrics were compared after aggregating the 15 m resolution data using a 5 × 5, or 75 m moving window. Previous research in the study area demonstrated that such aggregation provides the optimal relationship between ALS and SAR data while maintaining sufficient spatial detail in map products ([Mathieu et al., 2013; Naidoo et al., 2016; Urbazaev et al., 2015](#)). The relationship between HH and HV backscatter and ALS cover, and ALS volume, was investigated using a linear regression, a logarithmic model and the modified Water Cloud Model (WCM) ([Santoro et al., 2002](#)). Dry season SAR data from the years preceding the ALS data acquisition (2007, 2017) were also analyzed individually to check consistency of results.

The ALS cover and volume values were then predicted as a function of SAR backscatter using a simple inversion of the models. The models were developed on 70% of the data, while the remaining 30% of data were kept separate for validation purposes. A Bayesian inversion of the WCM (BWCM) was implemented following [Bouvet et al. \(2018\)](#). The BWCM requires inputs which estimate the standard deviation of the

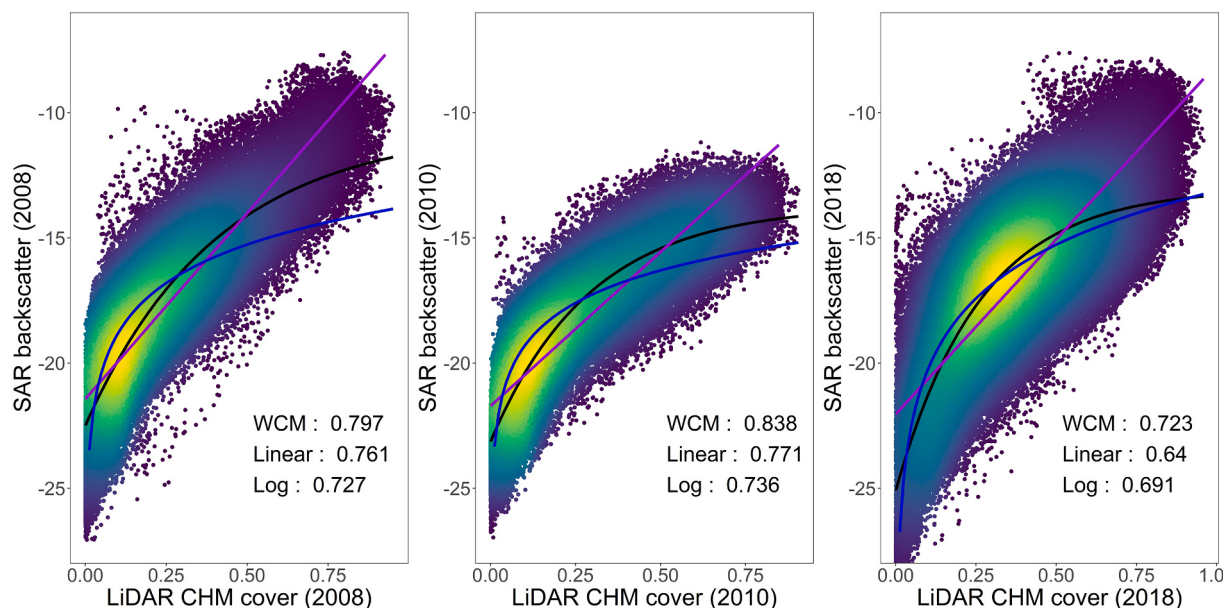


Fig. 3. Density plots of SAR HV backscatter and fractional cover derived from ALS LiDAR derived canopy height model (CHM). R^2 is given for the Water Cloud models (WCM, black), linear (purple) and logarithmic model (Log, blue). (For interpretation of the references to colour in this figure legend, the reader is referred to the web version of this article.)

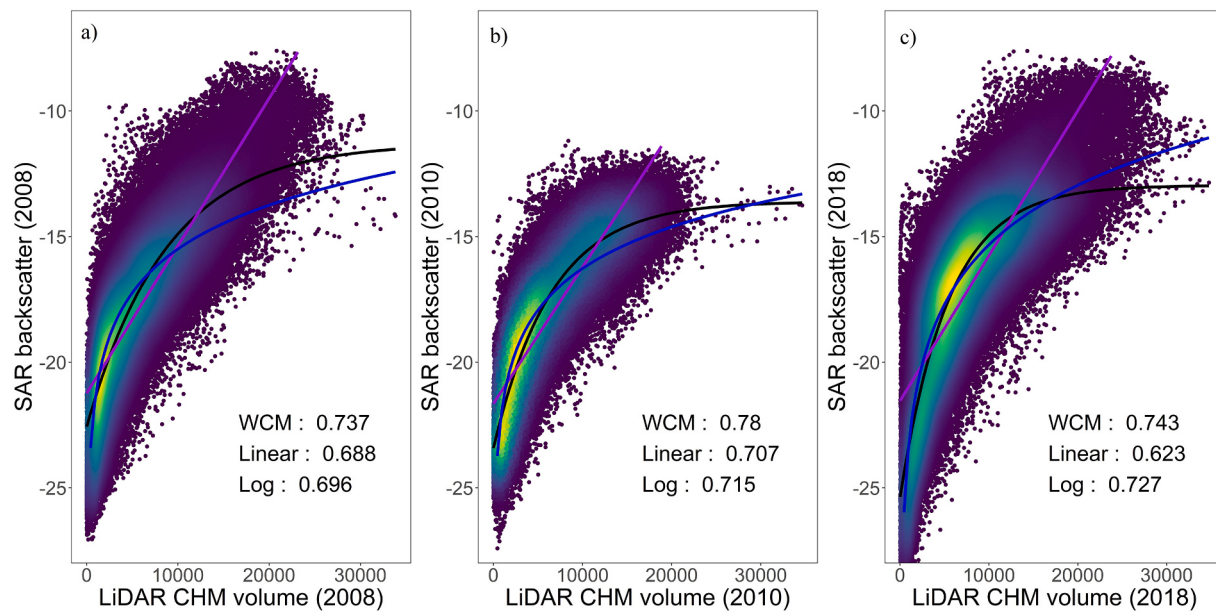


Fig. 4. Density plots of SAR HV backscatter and volume derived from ALS LiDAR derived canopy height model (CHM). R^2 is given for the Water Cloud models (WCM, black), linear (purple) and logarithmic model (Log, blue). (For interpretation of the references to colour in this figure legend, the reader is referred to the web version of this article.)

Table 2
Uncertainty assessment of inverted linear, logarithmic and Bayesian Water Cloud (BWCM) model predictions of volume for individual years.

| Year | Polarization | R^2 (linear) | Bias | %bias | RMSE | % RMSE |
|---------|--------------|-------------------|--------|--------|---------|-----------|
| 2007 | HV | 0.69 | -2.19 | -0.04 | 2450.46 | 47.10 |
| 2008 | HV | 0.69 | 1.06 | 0.02 | 2437.19 | 46.87 |
| 2010 | HV | 0.71 | -3.8 | -0.06 | 2403.42 | 43.19 |
| 2017 | HV | 0.63 | 1.68 | 0.02 | 2809.65 | 39.08 |
| 2018 | HV | 0.62 | -0.85 | -0.01 | 2866.00 | 39.85 |
| Average | | 0.67 | -0.82 | -0.014 | 2593.34 | 43.21 |
| Year | Polarization | R^2 (Log) | Bias | %bias | RMSE | RMSE |
| 2007 | HV | 0.74 | -16.14 | -0.31 | 2226.59 | 42.82 |
| 2008 | HV | 0.74 | -14.38 | -0.27 | 2225.96 | 42.78 |
| 2010 | HV | 0.76 | -19.84 | -0.35 | 2188.47 | 39.33 |
| 2017 | HV | 0.68 | -20.52 | -0.28 | 2604.01 | 36.21 |
| 2018 | HV | 0.67 | -20.63 | -0.28 | 2670.26 | 37.13 |
| Average | | 0.72 | -18.3 | -0.29 | 2383.05 | 39.65 |
| Year | Polarization | R^2 (BWCM) | Bias | %bias | RMSE | RMSE |
| 2007 | HH&HV | 0.75 | -1.89 | -0.03 | 2159.82 | 41.54 |
| 2008 | HH&HV | 0.75 | 1.36 | 0.02 | 2159.79 | 41.54 |
| 2010 | HH&HV | 0.77 | -0.28 | 0 | 2157.92 | 38.89 |
| 2017 | HH&HV | 0.7 | 0.23 | 0 | 2552.72 | 35.5 |
| 2018 | HH&HV | 0.68 | -0.76 | -0.01 | 2605.33 | 36.23 |
| Average | | 0.73 | -0.268 | 0 | 2327.11 | 38.74 |

backscatter for each cover or volume value that accounts for the backscatter variability with respect to other environmental conditions including surface moisture and surface roughness, as well as speckle noise. These standard deviation values were adapted from the standard deviation values of the backscatter expressed as a function of above-ground biomass used in Bouvet et al., 2018, which were obtained from electromagnetic modelling (Villard, 2009).

4.3. Estimation of cover change from SAR backscatter

Cover change was estimated from SAR backscatter data in two ways, (i) by directly estimating cover change from the backscatter change between two years ($\Delta\gamma^0$) (hereafter referred to as “direct backscatter

Table 3
Uncertainty assessment of inverted linear, logarithmic and Bayesian Water Cloud (BWCM) model predictions of cover for individual years.

| Year | Polarization | R^2 (linear) | Bias | %bias | RMSE | %RMSE |
|---------|--------------|----------------|-------|-------|------|-------|
| 2007 | HV | 0.75 | 0 | 0.026 | 0.09 | 41.45 |
| 2008 | HV | 0.76 | 0 | -0.03 | 0.08 | 40.82 |
| 2010 | HV | 0.77 | 0 | -0.04 | 0.09 | 39.83 |
| 2017 | HV | 0.64 | 0 | 0.11 | 0.11 | 34.91 |
| 2018 | HV | 0.64 | 0 | -0.02 | 0.11 | 35.12 |
| average | | 0.71 | 0 | -0.03 | 0.10 | 38.43 |
| Year | Polarization | R^2 (Log) | Bias | %bias | RMSE | %RMSE |
| 2007 | HV | 0.76 | 0.008 | 3.71 | 0.08 | 40.7 |
| 2008 | HV | 0.77 | 0.008 | 3.69 | 0.08 | 40.22 |
| 2010 | HV | 0.80 | 0.006 | 2.74 | 0.09 | 36.99 |
| 2017 | HV | 0.64 | 0.004 | 1.22 | 0.11 | 35.29 |
| 2018 | HV | 0.63 | 0.004 | 1.19 | 0.11 | 35.52 |
| average | | 0.72 | 0.006 | 2.51 | 0.09 | 37.74 |
| Year | Polarization | R^2 (BWCM) | Bias | %bias | RMSE | %RMSE |
| 2007 | HH&HV | 0.80 | 0 | 0.02 | 0.08 | 36.9 |
| 2008 | HH&HV | 0.81 | 0 | 0 | 0.07 | 36.21 |
| 2010 | HH&HV | 0.82 | 0 | 0 | 0.08 | 35.0 |
| 2017 | HH&HV | 0.64 | 0 | -0.04 | 0.11 | 35.0 |
| 2018 | HH&HV | 0.64 | 0 | 0.01 | 0.11 | 34.84 |
| average | | 0.74 | 0 | 0.01 | 0.09 | 35.59 |

change” approach), and (ii) by calculating cover change from the difference between SAR-derived cover products of individual years (hereafter referred to as “product difference” approach). The SAR predicted cover change was then compared to the ALS cover change (ΔC_{ALS}) to assess the reliability of these two approaches over the three time periods.

In the direct backscatter change approach, $\Delta\gamma^0$ is expressed as the ratio of backscatter intensities: $\Delta\gamma^0 = \gamma_2^0/\gamma_1^0$, where γ_1^0 and γ_2^0 represent the backscatter intensities in year 1 and 2, which is more adapted to the statistical distribution of the SAR intensities than the difference of the backscatter intensities $\gamma_2^0 - \gamma_1^0$ (Rignot and Van Zyl, 1993). Note that when expressed in dB, this backscatter ratio is equal to the difference of the backscatter intensities: $(\Delta\gamma^0) \text{ dB} = (\gamma_2^0) \text{ dB} - (\gamma_1^0) \text{ dB}$. Therefore, negative values of $(\Delta\gamma^0) \text{ dB}$ represent a decrease of the backscatter in time, which indicates a potential decrease in vegetation cover or volume, and positive values represent an increase. To reduce the impact of

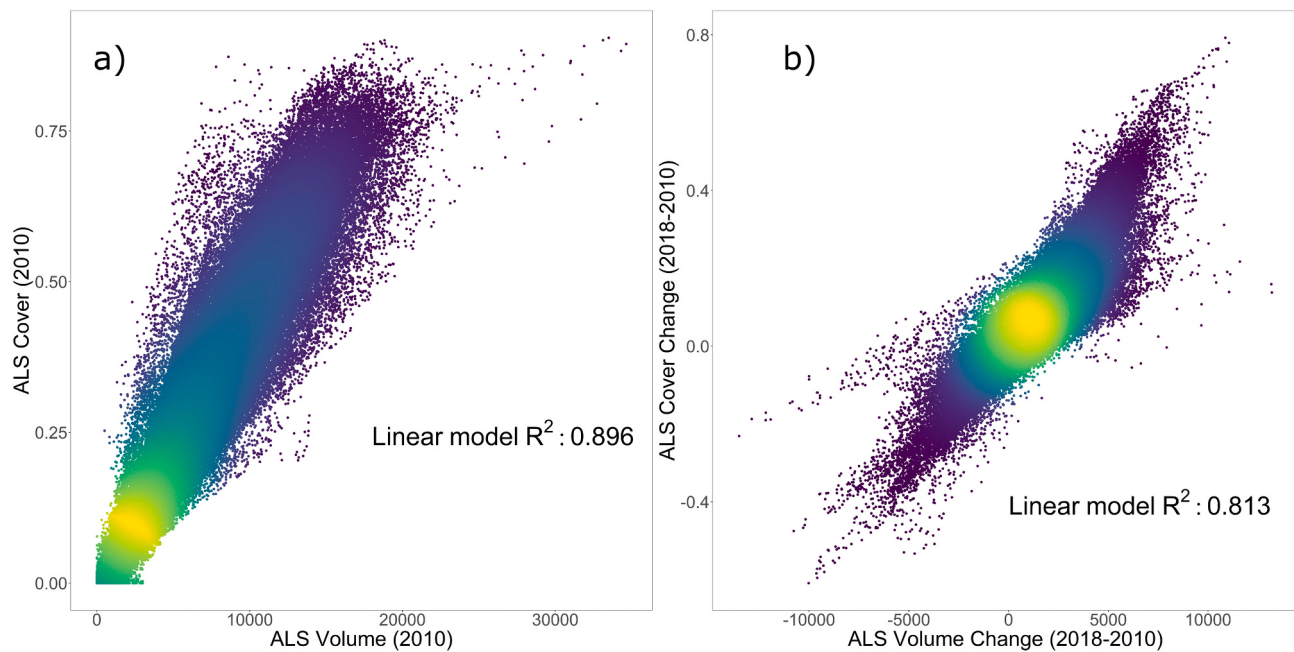


Fig. 5. (a) Density plot of ALS CHM 15 m aggregated cover vs. volume for 2010. (b) Density plot of ALS CHM-derived cover change vs. volume change for period 2018–2010.

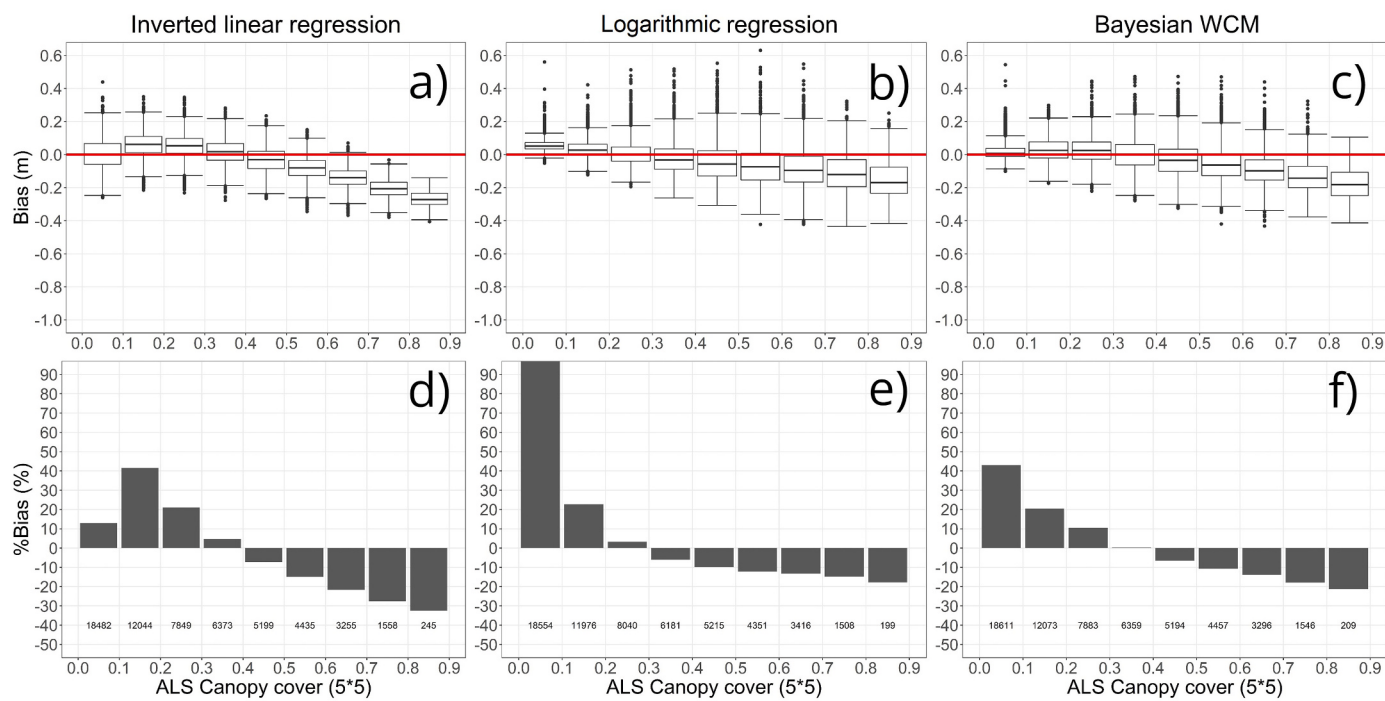


Fig. 6. Distribution of bias and % bias of cover prediction along cover range by linear, Log and BWCM models for 2010. (Plots for other years are near identical and given in supplementary materials)

the very large abundance of data with near zero cover change values on the models, the data were resampled by randomly selecting 100 samples from bins at increments of 0.01 ALS cover change. This bootstrapping process involved generating 100 different random sub-samples of data (with replacement) and fitting 100 models to calculate mean statistics. Finally, the relationship between $\Delta\gamma^0$ and ALS cover change (ΔC_{ALS}) was modelled using a linear function.

5. Results

5.1. Individual years: cover or volume vs. backscatter

Table 1 presents the coefficient of determination (R^2) of the relationships between backscatter (HH or HV) and vegetation parameters (volume or cover) using the linear regression, logarithmic model and WCM, for years 2007, 2008, 2010, 2017 and 2018. The R^2 measures the amount of variance in backscatter that is explained by the cover and

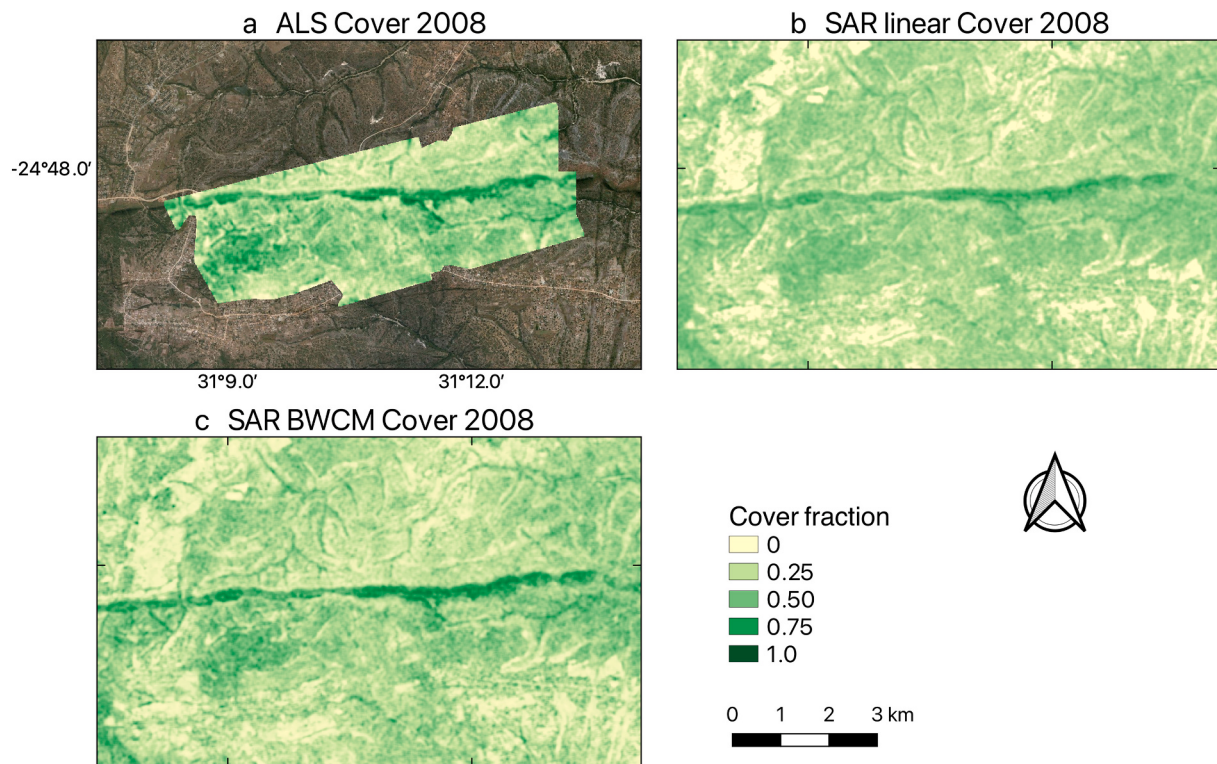


Fig. 7. Woody cover fraction for Agincourt site in study area derived from (a) ALS data (2008), (b) predicted with a Linear model and (c) BWCM model from HV ALOS PALSAR data (2008).

volume respectively.

Volume: The average R^2 of individual years using HH polarization was 0.63, 0.67 and 0.71 respectively for linear, log and WCM models (Table 1). Using HV polarization the average R^2 was 0.04 higher than for HH at 0.67, 0.71 and 0.75 for linear, log and WCM models respectively (Fig. 4).

Cover: The average R^2 of individual years using HH polarization was 0.66, 0.66 and 0.72 respectively for linear, log and WCM models (Table 1). The density plots indicate some level of saturation of backscatter with increased cover, especially in 2010, but otherwise a saturation effect was not apparent, as indicated by the strength of the linear model. Using HV polarization, the average R^2 was 0.05 higher than for HH at 0.71, 0.71 and 0.77 for linear, log and WCM models respectively (Fig. 3). Compared to volume, the R^2 values for cover were 0.04 (6%) and 0.02 (2.6%) higher for linear model and WCM respectively, in the case of HV. Overall, the strongest relationship was found between the HV backscatter and cover with the WCM model. Interestingly, 2007, 2008 and 2010 had consistently and notably higher R^2 than 2017, 2018. However, due to differing ALS extents, not all the years sampled the same sites and therefore they are not directly comparable.

5.2. Model predictions for individual years

Models for individual years were inverted to predict cover and volume from the backscatter, and validated using the 30% of data excluded from model development. For brevity, only HV results were presented for the linear and log models, while the BWCM used both HH and HV. These models were used to produce maps of cover or volume for the individual years.

Volume: The linear models had an average $R^2 = 0.67$, %bias = -0.014% , and %RMSE = 43.21%. The logarithmic models had an average $R^2 = 0.72$, %bias = -0.29% , and %RMSE = 39.65%. The BWCM had a slightly higher average $R^2 = 0.73$, a small %bias = 0.0%, and lower %RMSE = 38.74% (Table 2).

Cover: The linear models had an average $R^2 = 0.71$, %bias = 0%, RMSE = 0.10 and %RMSE = 38.4%. The logarithmic models had an average $R^2 = 0.72$, %bias = 0.006%, RMSE = 0.09 and %RMSE = 37.74%. The BWCM had a higher average $R^2 = 0.74$, %bias = 0.01%, and lower RMSE = 0.09, %RMSE = 35.59% (Table 3). The predictions for 2007 and 2008 and 2010, corresponding with PALSAR had notably higher R^2 ($> +0.12$) and lower RMSE than those of 2017, 2018 which used PALSAR-2 data. However, it should be noted that these two epochs included data from different combinations of sites and thus data, which may explain differences (Fig. 1). Overall, cover was predicted slightly better than volume, but otherwise the results were very similar.

5.3. Relationship between ALS CHM-derived cover and volume

Given that results for volume and cover were very similar, the relationship between these two structural metrics was explored using the aggregated 15 m CHM. The linear relationship between cover and volume was very strong with R^2 of 0.92, 0.90 and 0.86 for 2008, 2010 and 2018 respectively (Fig. 5a, example 2010). This relationship is primarily a function of taller trees typically having a larger crown diameter, whereas shrubs tend to have dense cover but lower height and subsequent volume. This strong relationship (Fig. 5a) illustrates that these two, ALS derived, structural metrics are highly correlated at 15 m aggregation. Similarly, ALS cover change and volume change between years were also highly correlated with R^2 above 0.8 (Fig. 5b). Therefore, for brevity, the remainder of the paper mainly reports results for cover since the results for volume were nearly identical.

5.4. Bias distribution of model predictions for individual years

The bias of cover estimation with SAR was analyzed (using the 30% validation data) across the entire range of cover values to determine any trends and differences in the bias between models. All three the main years under investigation (2008, 2010, 2018), showed very similar

results and therefore only 2010 was given as example here (Fig. 6), while the graphs for 2008 and 2018 are given in supplementary material (Figs. S1 and S2). The linear model primarily overestimated in the 0.1–0.2 cover range, but the overestimation stayed below +0.1 cover (Fig. 6a,d). Underestimation gradually increased with cover to −0.2 and −0.3 at high cover of 0.7–0.9. The Log and BWCM models had very similar bias distributions. The bias varied in magnitude between years but maintained the same general pattern (Figs. S1 and S2). Within very sparse cover ranges of 0 to 0.1 there was a bias of +0.05 leading to a very high %bias of up to 100% (Fig. 6e,f). The lowest cover bias of +10% and −10% occurred between 0.2 and 0.4 cover where majority of the data resides. The underestimation increases with cover from %bias of −10% to −30% between cover of 0.4 and 0.8. The negative bias however remained less than −0.2 for cover below 0.8. Compared to the Linear model, the BWCM underestimates considerably less at high cover, but overestimates in the very low cover ranges (< 0.1).

5.5. SAR vs. ALS cover maps for individual years

The maps of cover, predicted by the BWCM, closely matched the patterns of cover in the ALS data (Fig. 7). The linear model

Table 4
R² and RMSE of linear relationship between backscatter change and ALS cover change, and volume change without resampling of data (all data included).

| Year2 | Year1 | Parameter | Polarization | Linear R ² | RMSE |
|-------|-------|-----------|--------------|-----------------------|--------|
| 2018 | 2008 | volume | HV | 0.207 | 2009.1 |
| 2018 | 2010 | volume | HV | 0.337 | 1586 |
| 2010 | 2008 | volume | HV | 0.159 | 1270.9 |
| 2018 | 2008 | cover | HV | 0.161 | 0.119 |
| 2018 | 2010 | cover | HV | 0.359 | 0.096 |
| 2010 | 2008 | cover | HV | 0.15 | 0.06 |
| 2018 | 2008 | volume | HH | 0.185 | 2027.9 |
| 2018 | 2010 | volume | HH | 0.293 | 1644.2 |
| 2010 | 2008 | volume | HH | 0.135 | 1290.3 |
| 2018 | 2008 | cover | HH | 0.154 | 0.119 |
| 2018 | 2010 | cover | HH | 0.312 | 0.099 |
| 2010 | 2008 | cover | HH | 0.13 | 0.06 |

underestimated high cover (Fig. 7b) and had limited differentiation in the midrange values compared to the ALS data and BWCM. The SAR-derived cover maps did not overestimate cover along the steep ridge in the center of the map compared to the ALS cover, suggesting that the topographic correction to γ^0 was effective.

5.6. Cover change between years

5.6.1. Change in SAR backscatter vs. change in ALS cover

Given that the vast majority of the data were clustered around zero change in ΔC_{ALS} and zero $\Delta \gamma^0$, this resulted in a weak positive linear relationship with R² at 0.13–0.37 for HV and 0.13 to 0.31 for HH (Table 4). However, since the hyper-abundant no-change data points were of less interest than the data containing actual cover change, the imbalance in the data density was addressed by randomly selecting 100 samples from ΔC_{ALS} bins at 0.01 increments from 70% of the data, repeated 100 times. This bootstrapping helped elucidate the relationship and resulted in considerable increases in R² to 0.41 (2010–2008), 0.4 (2018–2008) and 0.7 (2018–2010) (Fig. 8) (Table 5). However, given that the subsampling radically reduced data points with values close to zero (no change), the RMSE's increased by an average of 65%. These models were inverted in order to predict cover change directly from backscatter change ($\Delta \gamma^0$).

Reductions in cover, such as −0.3 to −0.4, were associated with 1–4 dB reductions in HV backscatter. In contrast, cover increases of +0.4 to +0.6 caused an increase in HV backscatter of 3–5 dB (Figs. 8 b,c, Supplementary Material S6 b,c). The slopes of the inverted linear models (constrained to intercept the origin) indicate that 1 dB $\Delta \gamma^0$ corresponded to 0.093, 0.099 and 0.053 cover change respectively for 2018–2010, 2018–2008 and 2010–2008 respectively (Figure Supplementary Material S3). The short period between 2008 and 2010 contained limited ΔC_{ALS} and $\Delta \gamma^0$, as could be expected (Fig. 8a). The period 2018–2010 contained more change than 2018–2008 (Fig. 8b,c), which may be unexpected, however this could be attributed to the fact that the two periods contain different combinations of sites and ALS extents, which experienced different rates of cover change (Fig. 1). The results of the three periods are therefore not directly comparable.

T-tests were conducted to test whether specific ranges of positive and

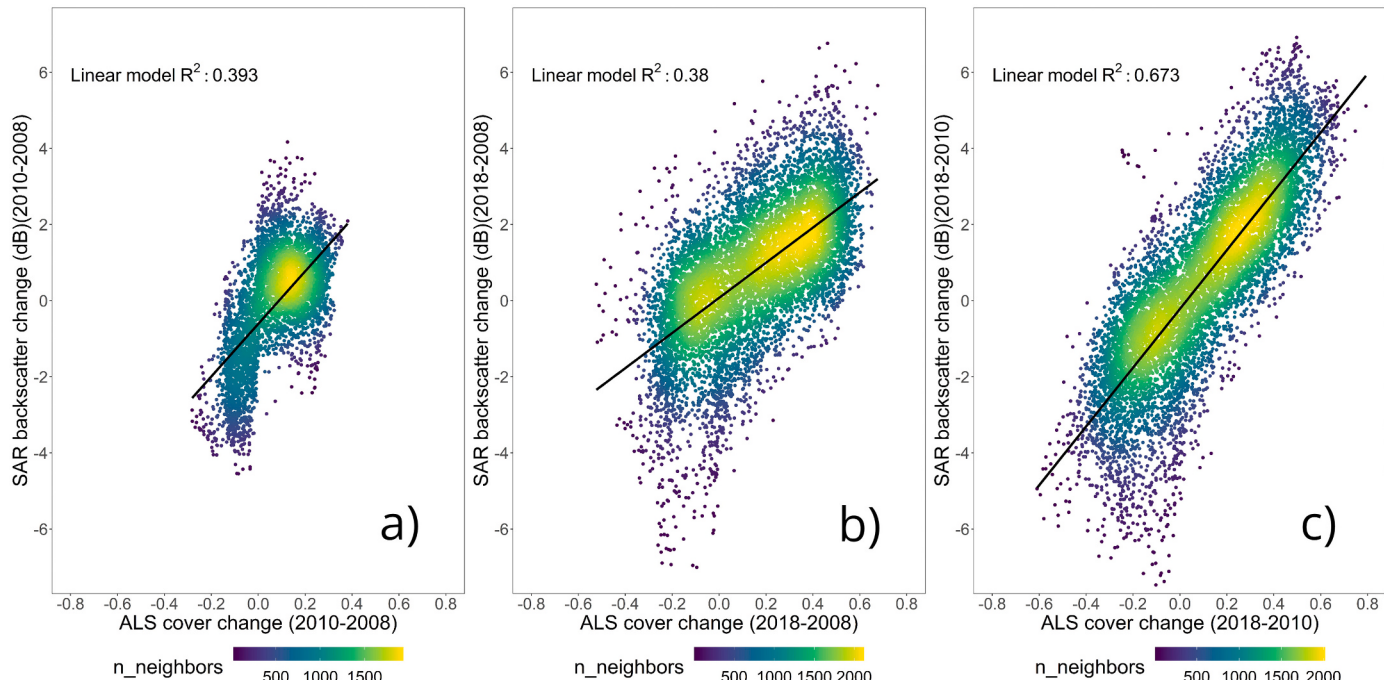


Fig. 8. HV SAR backscatter change ($\Delta \gamma^0$) vs. ALS CHM cover change (ΔC_{ALS}) for three time periods. Data were sub-sampled by randomly selecting 100 samples for every 0.01 ΔC_{ALS} increment. (Plots are based on one of 100 resampled datasets used to calculate the mean R²).

Table 5

R^2 and RMSE of linear relationship between backscatter change and ALS cover change and volume change with resampling of data. R^2 and RMSE values given are the means of 100 repetitions using subsamples of the data.

| Year2 | Year1 | Parameter | Polarization | Linear R^2 | RMSE |
|-------|-------|-----------|--------------|--------------|--------|
| 2018 | 2008 | volume | HV | 0.396 | 3484.2 |
| 2018 | 2010 | volume | HV | 0.553 | 2717.8 |
| 2010 | 2008 | volume | HV | 0.372 | 2220.8 |
| 2018 | 2008 | cover | HV | 0.399 | 0.196 |
| 2018 | 2010 | cover | HV | 0.697 | 0.153 |
| 2010 | 2008 | cover | HV | 0.4 | 0.105 |
| 2018 | 2008 | volume | HH | 0.33 | 3668.1 |
| 2018 | 2010 | volume | HH | 0.536 | 2769.1 |
| 2010 | 2008 | volume | HH | 0.341 | 2286.4 |
| 2018 | 2008 | cover | HH | 0.306 | 0.21 |
| 2018 | 2010 | cover | HH | 0.664 | 0.161 |
| 2010 | 2008 | cover | HH | 0.353 | 0.11 |

negative cover changes ($-0.5 \sim -0.25$, vs. $+0.25 \sim +0.5$) could be distinguished from each other based on the magnitude of $\Delta\gamma^0$ (Table 6) (Fig. S4 supplementary material). The t-tests were repeated 100 times on the sub-sampled data and the mean p -values were used to determine statistical significance between classes (Table 6). All of the ALS cover change classes differed significantly from each other, with the exception of two cases, e.g. $-0.25 \sim -0.05$ and $-0.05 \sim +0.05$ for both 2018–2008 and 2018–2010. Note that cover changes of >0.5 generally did not have enough data samples to allow a valid test for significant differences with other classes. The 2018–2010 period and associated sites had the largest differences in the mean backscatter of classes, e.g. -2.6 dB change for $-0.5 \sim -0.25$ and $+2.45$ dB change for $+0.25 \sim +0.5$ (Table 6). Overall, even moderate positive and negative changes in cover of 0.25 to 0.5, could be discerned by $\Delta\gamma^0$.

5.6.2. SAR-predicted cover change vs. ALS cover change

Cover change was predicted by the inverted models, namely (i) direct backscatter change ($\Delta\gamma^0$) model, (ii) BWCM product difference and (iii) the Log model product difference. These cover change predictions were compared using the 30% data that were not used in model development (Fig. 9). Overall, the BWCM had the highest R^2 for all years, 0.79 for 2018–2010, 0.47 for 2018–2008, and 0.56 for 2010–2008, followed by the Log model which consistently had notably higher R^2 values than the direct backscatter change model (Table 7). The direct backscatter change model, on the other hand, generally had the lowest RMSE values of 0.196, 0.152 and 0.104 for 2018–2008, 2018–2010 and 2010–2008, respectively. The direct backscatter change

model furthermore had a linear relationship that was better centered around the 1:1 line with a mean bias = 0 (Fig. 9 b,c), while the other two product difference models deviated notably from the 1:1 line with weaker slopes that indicated over and under estimation at low and high ends, respectively (Fig. 9e,f,h,i). The results suggest that the SAR-derived cover change products can predict cover change, but they clearly underestimate the magnitude of the change equally on both the negative and positive ends of the change range (Fig. 9e,f,h,i). For any given ALS change range for 2018–2010, e.g. $-0.3 \sim -0.4$, the BWCM predicted a range of cover changes of $-0.1 \sim -0.3$, with a mean of approximately -0.2 . Similarly, positive cover changes showed equivalent patterns of underestimation. The bias of the models is discussed in detail in the next section.

5.6.3. Bias of SAR-predicted cover change

The distribution of bias for the three cover change prediction models were analyzed across the range of ΔC_{ALS} based on the entire 30% validation data set (Fig. 10). All the SAR-derived change predictions consistently underestimated positive and negative change compared to ΔC_{ALS} . When comparing the %bias of the cover change estimates of BWCM to that estimated by the direct backscatter change model, the latter had significantly lower %bias in 2018–2010 (Fig. 10f,l). More specifically, the underestimation of positive change by the direct backscatter model was less than half that of the BWCM model. This is in line with the observation of a 1:1 relationship for the unbiased direct backscatter model in Fig. 9. Low levels of change of $-0.2 \sim +0.2$, had low absolute biases, but the %bias was high. These very low levels of change are, however, of minor interest from a monitoring perspective and the %bias was exaggerated as change values approached zero. Both positive and negative changes of 0.2 to 0.6 were underestimated at a consistent level 50–60% by the BWCM (Fig. 10l). The magnitude of underestimation of change (%bias) for 2018–2008 was twice that of 2018–2010 (Fig. 10).

5.6.4. SAR-derived cover change maps

This section provides examples of SAR-derived cover change maps using various models without claiming that one model output was superior to another as most models produced similar maps with subtle differences. The BWCM cover change map for 2008–2010 showed no change over the majority of the ALS sites, as could be expected during the limited 2-year period (Fig. 11). However, specific areas did show significant negative changes that were detected by both the ALS and SAR BWCM products. For example, illegal logging of a stand of large knob thorn trees (*Senegalia nigrescens*) was detected in site 1 (Fig. 11) in the

Table 6

Results of t-test for significant differences in the mean backscatter changes ($\Delta\gamma^0$) between various cover change classes. t-tests were repeated on each of the 100 subsamples. The p -values, mean γ^0 and STD were calculated from the mean class values of 100 sub-samples. Note: *****, ***, ** represent p-value of 0.0001, 0.001, 0.01. ns denotes no significant difference in $\Delta\gamma^0$.

| Cover change classes | NA | $-0.25 \sim -0.05$ | $-0.05 \sim 0.05$ | $0.05 \sim 0.25$ | $0.25 \sim 0.5$ | Mean (STD) |
|----------------------|-------------------|--------------------|-------------------|------------------|-----------------|-------------------|
| 2010–2008 | | | | | | |
| $-0.25 \sim -0.05$ | | | | | | $-1.68 (1.16)$ |
| $-0.05 \sim 0.05$ | | **** | | | | $0.01 (1.33)$ |
| $0.05 \sim 0.25$ | | **** | *** | | | $0.62 (1.14)$ |
| $0.25 \sim 0.5$ | | **** | *** | ns | | $0.81 (0.84)$ |
| 2018–2008 | $-0.5 \sim -0.25$ | $-0.25 \sim -0.05$ | $-0.05 \sim 0.05$ | $0.05 \sim 0.25$ | $0.25 \sim 0.5$ | Mean (STD) |
| $-0.5 \sim -0.25$ | | | | | | $-1.17 (1.48)$ |
| $-0.25 \sim -0.05$ | **** | | | | | $-0.25 (1.51)$ |
| $0.05 \sim 0.05$ | ** | ns | | | | $-0.54 (2.03)$ |
| $0.05 \sim 0.25$ | **** | **** | **** | | | $1.01 (1.5)$ |
| $0.25 \sim 0.5$ | **** | **** | **** | *** | | $1.73 (1.17)$ |
| 2018–2010 | $-0.5 \sim -0.25$ | $-0.25 \sim -0.05$ | $-0.05 \sim 0.05$ | $0.05 \sim 0.25$ | $0.25 \sim 0.5$ | Mean (STD) |
| $-0.5 \sim -0.25$ | | | | | | $-2.35 (1.28)$ |
| $-0.25 \sim -0.05$ | **** | | | | | $-1.28 (1.55)$ |
| $0.05 \sim 0.05$ | **** | ns | | | | $-0.92 (1.62)$ |
| $0.05 \sim 0.25$ | **** | **** | **** | | | $1.06 (1.3)$ |
| $0.25 \sim 0.5$ | **** | **** | **** | **** | | $2.33 (1.19)$ |

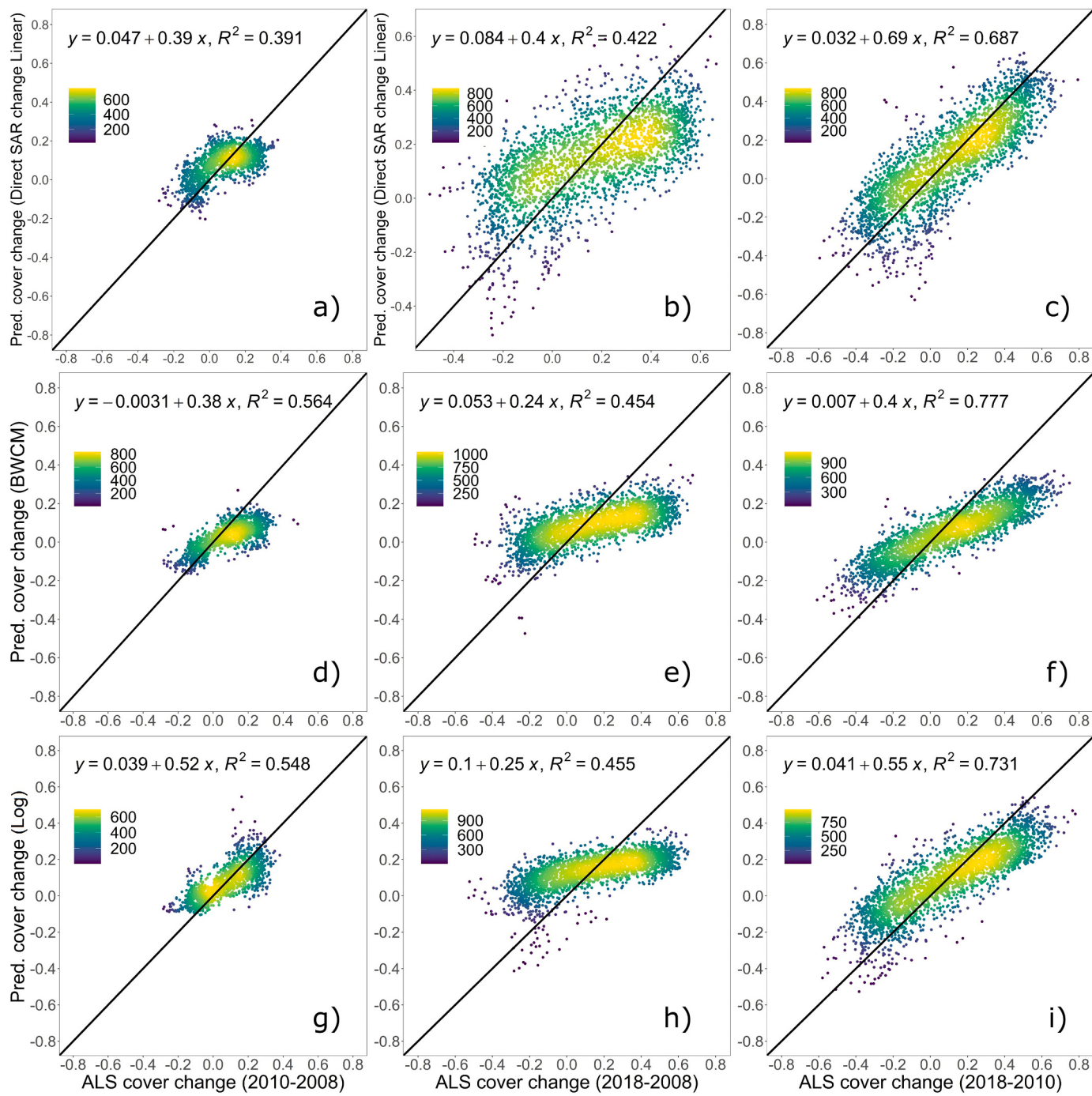


Fig. 9. Cover change predicted (y-axis) by direct backscatter change model (top panels), BWCM (middle panels), Log model (bottom panels) versus ALS cover change (x-axis). (Graphs represent one of 100 subsampled datasets).

communal rangelands, in the ALS data and then confirmed during a field visit (Fig. 11c,d). Site 2 (Fig. 11a,b) is a location inside Sabi Sands Nature Reserve where stands of large trees were lost due to elephant damage followed by wildfire which was also confirmed in the field in 2011 (see Discussion). Areas in the western part of the ALS data show significant increases in woody cover of up to +0.35, likely due to shrub encroachment. This increase was detected, but its magnitude was underestimated by the SAR change products.

The SAR-based cover change maps, e.g. BWCM map for 2010–2018 detected the loss of woody cover of up to −0.4 inside the former Andover nature reserve due to timber removal of large trees (>5 m in height according to ALS CHM), while the ALS detected a cover decrease up to

−0.6 (site 1, Fig. 12). In contrast, significant shrub encroachment occurred along the eastern boundary of Andover reserve in neighboring communal rangelands (site 2), resulting in a clear fence-line effect with up to +0.35 and +0.65 increase in cover predicted by the BWCM and ALS change products, respectively. The SAR-based cover change product therefore again underestimated the magnitude of the change. The ALS CHM data inspection confirmed that the shrubs <3 m in height in 2010 grew >70% in height by 2018.

The long-term cover change maps (e.g. BWCM, not shown), as well as the mosaiced $\Delta\gamma^0$ images, captured distinct fence-line contrasts between the communal areas, which generally displayed increases in woody cover and backscatter (west), and the conservation areas that displayed

Table 7

R^2 , Bias and RMSE for the three models predicting cover change. (Results are based on mean of 100 subsamples).

| Year2 | Year1 | Model | R^2 | Mean Bias | RMSE |
|-------|-------|---------------|--------------|-----------|--------------|
| 2018 | 2008 | Direct linear | 0.393 | 0 | 0.196 |
| 2018 | 2010 | Direct linear | 0.7 | 0 | 0.152 |
| 2010 | 2008 | Direct linear | 0.404 | 0 | 0.104 |
| mean | | | 0.499 | | 0.15 |
| 2018 | 2008 | BWCM | 0.47 | -0.054 | 0.21 |
| 2018 | 2010 | BWCM | 0.785 | -0.049 | 0.177 |
| 2010 | 2008 | BWCM | 0.566 | -0.045 | 0.107 |
| mean | | | 0.607 | | 0.164 |
| 2018 | 2008 | Log | 0.451 | -0.004 | 0.203 |
| 2018 | 2010 | Log | 0.741 | -0.002 | 0.152 |
| 2010 | 2008 | Log | 0.549 | 0.004 | 0.092 |
| mean | | | 0.58 | | 0.149 |

a general decrease in cover and backscatter (east) (Fig. 13, sites 1–3). This pattern was especially evident along the western boundary of the Manyeleti Game Reserve and the neighboring communal rangelands around the village of Welverdiend (Fig. 13, sites 1 and 2). Areas of $\Delta\gamma^0$ decreases coincided with lower woody cover inside the reserve compared to communal areas, which is visible in recent high-resolution optical images (Fig. 13b,c). This pattern continued along the entire length of the Manyeleti Reserve and parts of the boundary with the larger Sabi Sands Reserve further south (Fig. 13, site 3 near Justicia). The likely causes of this fence-line pattern are elaborated on in the Discussion.

6. Discussion

The collection of multi-date ALS data, initiated over a decade ago in the Lowveld of South Africa, (Asner et al., 2009; Wessels et al., 2011) provided a rare opportunity to quantify the ability of L-band SAR to track long-term changes in savanna vegetation structure and this study is the first to do so, to our knowledge. Repeat ALS data are very scarce, especially in Africa and this has constrained the ability to investigate the sensitivity of multi-date SAR data to detecting changes in savanna vegetation structure (Cartus et al., 2018; Odipo et al., 2016).

The relationship between PALSAR backscatter and volume or cover was first investigated for individual years, using various models, i.e., linear, logarithmic (Log) and WCM (Fig. 2). The results largely confirmed previous findings in the same study area (Mathieu et al., 2013; Naidoo et al., 2016; Urbazaev et al., 2015). As previously demonstrated, the cross-polarised HV backscatter produced a higher average R^2 in relation to volume than HH, at 0.71 and 0.75 for Log and WCM models respectively. Cover showed a slightly stronger relationship with HV backscatter than volume did, with a mean R^2 of 0.71 and 0.77 for Log and WCM models respectively. Overall, the WCM model, based on HV backscatter, had the strongest relationship with cover (Fig. 3). In contrast, Naidoo et al., 2015 found a slightly stronger relationship with volume than cover in the same study area, with R^2 of 0.79 and 0.77 respectively, however, this minor difference in the results could be attributed to a different modelling approach (random forest was used in Naidoo's study).

Among the cover prediction models, the BWCM performed slightly better than the Log model with average $R^2 = 0.74$, %bias = 0.01%, and RMSE = 0.09 (%RMSE = 35.59%). Even though the BWCM included both HH and HV polarizations and accounts for the backscatter variability, partially caused by other environmental conditions (Bouvet et al., 2018), it did not significantly outperform the simple HV-based Log model. This could be explained by the fact that the vegetation's structural parameter values in these landscapes remained below the saturation level of the backscatter vs. cover (or volume) relationship, and in this range of values, the Log and BWCM models performed very similarly. The results were a notable improvement over our previous study that predicted cover in arid savannas of northern Namibia with $R^2 =$

0.65 and RMSE = 0.16, using ALOS PALSAR-2 global mosaics and random forest models based on ALS training data (Wessels et al., 2019). The improved results could be attributed to multiple factors, such as i) a smaller study area with less diverse savanna types and relatively flat terrain, ii) a smaller temporal gap between the dates of the ALS and PALSAR or PALSAR-2 data, iii) custom selection of dry season ALOS PALSAR imagery and (iv) the implementation of custom image pre-processing that included multi-date speckle filtering (Quegan and Yu, 2001).

The bias distribution for individual years were very similar for the Log and BWCM models. The lowest bias of +10% and -10% occurred between 0.2 and 0.4 cover where the majority of the data occurred. The underestimation increased with cover, from a %bias of -10% to -30% for cover between 0.4 and 0.8. The underestimation of cover or biomass at the higher end of the data range by SAR-based models, is well-documented (Rodríguez-Veiga et al., 2019; Wessels et al., 2019; Yu and Saatchi, 2016), and is caused by the saturation of L-band backscatter with increased biomass levels above 90–110 Mg ha (Yu and Saatchi, 2016). However, saturation is unlikely to be the cause in the current study, as biomass in savannas is seldom above 60 Mg/ha (Colgan et al., 2013; Hensley et al., 2013; Odipo et al., 2016; Wingate et al., 2018). The underestimation is more likely caused by the well-established statistical process known as attenuation or regression dilution that causes the bias, resulting from random error in the independent variable which causes the ordinary least squares (OLS) determined slope to tend toward zero (Fuller, 2009; Rejou-Mechain et al., 2014). Alternatives to OLS, such as Reduced Major Axis regression and Theil-Sen slope estimator have been proposed for developing models estimating biophysical variables from remote sensing data (Rejou-Mechain et al., 2014).

The cover and volume metrics derived from CHMs were highly correlated at 15 m aggregation, with R^2 of 0.86–0.92 (Fig. 5), which explains why all results for the two metrics were very similar. The ALS cover change and volume change between pairs of years were furthermore also highly correlated, with R^2 above 0.8, suggesting that further evaluating both metrics would be redundant. It was initially expected that $\Delta\gamma^0$ should have a stronger relationship with volume change than cover change, as woody vegetation volume should have a stronger relationship with volume scattering (Clark et al., 2011; Dobson et al., 1992) and should account for the influence of height, as vegetation transmissivity increases with decreasing height and vertical vegetation thickness (Cartus et al., 2018). However, it was not the case in the current study as woody vegetation was generally much lower (< 6 m) than the 5–20 m high, sparse forests used during modelling cover change detection by (Cartus et al., 2018). The subsequent results discussed for cover change therefore apply equally to volume change in these short stature savannas. The units of fractional cover change are furthermore easier to interpret than units of volume change, especially in the maps of change.

The linear relationship between $\Delta\gamma^0$ and ΔC_{ALS} varied between year pairs and the associated ALS sites but reached a maximum R^2 of 0.7 for 2018–2010 and a moderate R^2 of 0.4 for 2018–2008 (Fig. 8). These pairwise models were inverted to the direct backscatter change ($\Delta\gamma^0$) model to predict cover change. Significant reductions in cover of -0.3~−0.4 were associated with a 1–4 dB reduction in HV γ^0 , while cover increases of +0.4~+0.6 resulted in increases of 3–4 dB. The slopes of the inverted linear models (constrained to intercept the origin) indicate that 1 dB $\Delta\gamma^0$ corresponded to approximately 0.1 cover change for 2018–2010, 2018–2008. Note that this slope, or cover change per 1 dB $\Delta\gamma^0$, may be underestimated due to the regression dilution bias discussed above (Fuller, 2009; Rejou-Mechain et al., 2014), as well as smoothing caused by the 5 × 5 aggregation of $\Delta\gamma^0$ and ΔC_{ALS} . A t-test revealed that all of the ALS cover change classes differed significantly from each other, with the exception of two cases, (-0.25~−0.05 and −0.05~+0.05 in two-year pairs). Relatively subtle cover changes had significantly different $\Delta\gamma^0$, e.g. -2.6 dB change for -0.5~−0.25 cover change and +2.45 dB change for +0.25 to +0.5 cover change. This suggests that $\Delta\gamma^0$ can be

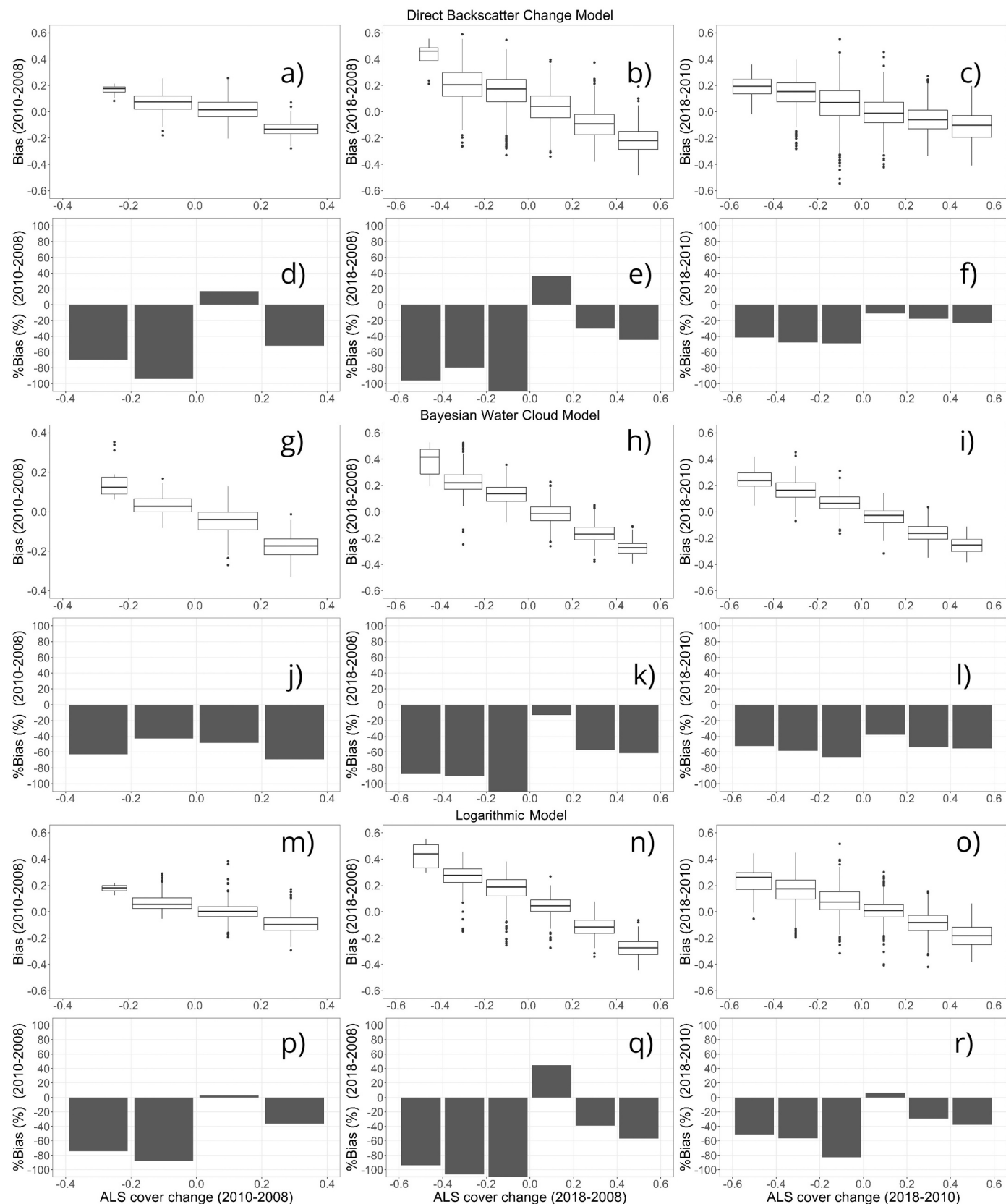


Fig. 10. Bias and %bias of direct backscatter model (a-f), BWCM (g-i) and Log model (m-r) in predicting cover change within ALS cover change bins for three pairs of years.

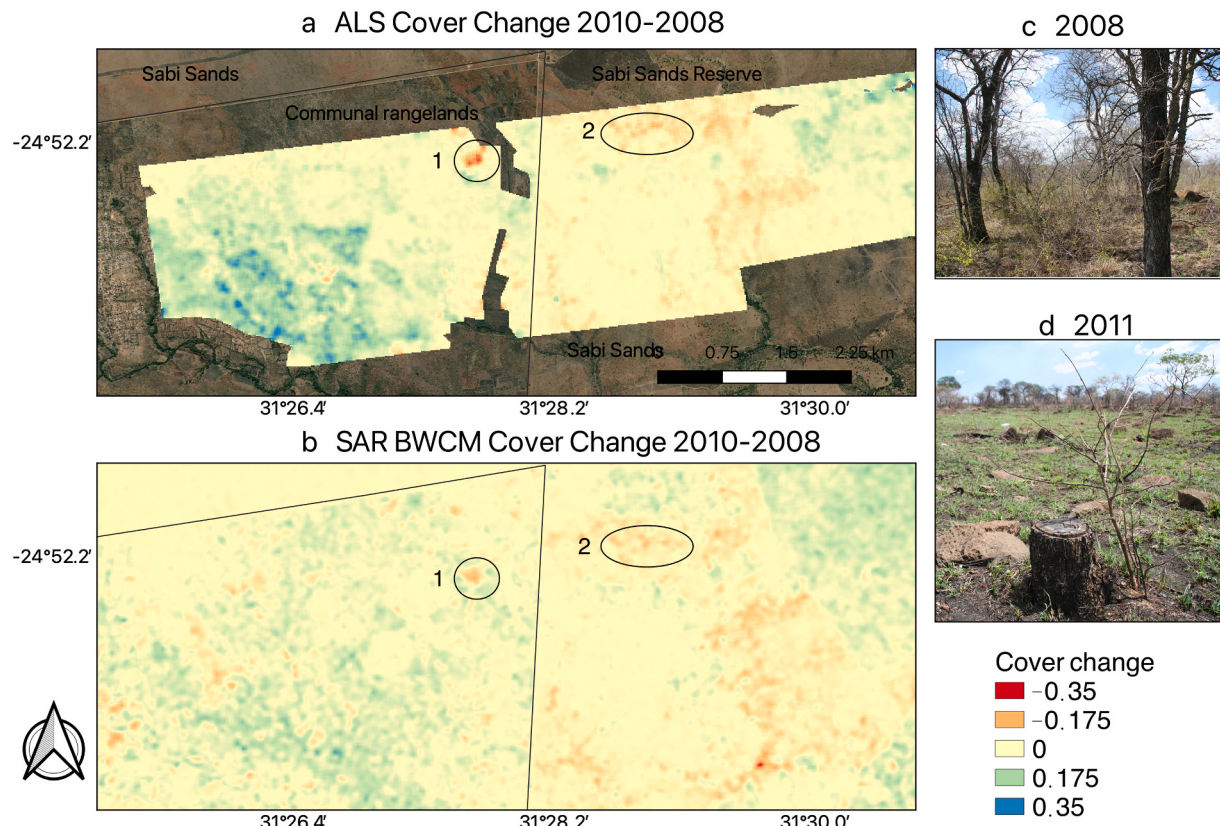


Fig. 11. Cover change between 2008 and 2010 in Sabi Sands Nature Reserve (SSNR) and neighboring communal rangelands derived from (a) ALS data aggregated to $15 \text{ m} \times 15 \text{ m}$ cover change and (b) SAR-based predicted cover change using BWCM. Site 1 was the location of illegal clear cut with (c) intact trees in 2008 and (d) clear cut in 2011. Site 2 in SSNR experienced the loss of big trees.

used with confidence to directly map distinct cover change classes of ± 0.25 and ± 0.5 and most likely >0.5 change. If we express these cover changes as a rate over, for example, 10 years, this would amount to ± 0.025 , ± 0.05 and > 0.05 fractional cover change per year, respectively. Several studies working in lower biomass woodlands in Africa have used a variety of methods to suggest that L-band SAR could detect relatively subtle biomass changes ($< 30 \text{ Mg/ha}$) (Mitchard et al., 2013; Odipo et al., 2016; Ryan et al., 2012; Wessels et al., 2019). Using a forest cover change error model, Cartus et al., 2018 found that L-band HV backscatter should be able to detect 50% cover change at hectare scale in mature forests, but would be unlikely to detect 50% cover change at lower 5 m heights of 5 m (similar to savannas), as error probability increases with decreasing height. The present study found that that L-band backscatter had a higher sensitivity to change in short stature, low biomass savannas ($< 50 \text{ Mg/ha}$) than predicted by Cartus et al. (2018), as it was able to distinguish cover change at 0.25 increments. This holds significant potential for monitoring vegetation structural change to inform long-term management decisions in savannas, as discussed below. It furthermore suggests that the planned L-band NASA ISRO SAR (NISAR) mission should be able to meet the mission requirement of detection disturbances of $>50\%$ canopy cover change with 80% accuracy (NISAR, 2018). The high sensitivity achieved in this study could be due to the careful selection of dry season ALOS imagery (with similar incidence angles) to avoid soil and canopy moisture variability which are known to cause significant variability in backscatter, especially in more open forested landscapes such as boreal forests (Cartus et al., 2014; Huuva et al., 2020; Mitchard, 2009; Lucas et al., 2010) or savanna woodlands (Bouvet et al., 2018; Mathieu et al., 2013).

ALS data were collected for specific sites in different combinations of years (Fig. 1) and consequently the prediction models trained on the ALS data were different, leading to different levels of uncertainty between

years and change pairs. The model development was therefore highly dependent on the location, characteristics and representativeness of the ALS training data within the broader study region. Thus, while the coverage of the repeat ALS data was extensive and unique in this study area, it was not necessarily sufficient to derive universally applicable models, which potentially limits the reliable regional application of the current models (Huuva et al., 2020). This dependence on finite training data for model development, however, remains one of the most vexing limitations of regional remote sensing applications in general.

When comparing the three different cover change prediction models to the Δ_{ALS} , the BWCM had the highest mean R^2 of 0.59, while the Log and direct backscatter change model both had lower mean RMSE's of 0.15 (Table 7). The models therefore had similar performance with no single model consistently producing a higher R^2 and lower RMSE. Although the uncertainty (RMSE) of annual cover maps was expected to aggregate when calculating cover change using the product difference approach (BWCM and Log models) (Huuva et al., 2020), the RMSE's were not higher than that of the direct backscatter change approach. When considering all three change prediction methods and year pairs, the mean RMSE was 0.15 (STD = 0.045), which is 7.7% of the total potential cover change range (-1.0 to $+1.0$) and 13% of the observed cover change range (-0.6 to $+0.6$). An uncertainty level of 7–13% on cover change should be acceptable for long-term monitoring and should allow confident decision making in savannas. The direct backscatter change model had a clear 1:1 linear relationship with Δ_{ALS} , while the two product difference models had significant overestimation at the low end and underestimation of cover change at the high end of the range. The underestimation of positive change (%bias) by the direct backscatter model was less than half that of the BWCM model for 2018–2010 and 2018–2008 (Fig. 10). The results for the three cover change prediction models were very similar, however the direct backscatter change

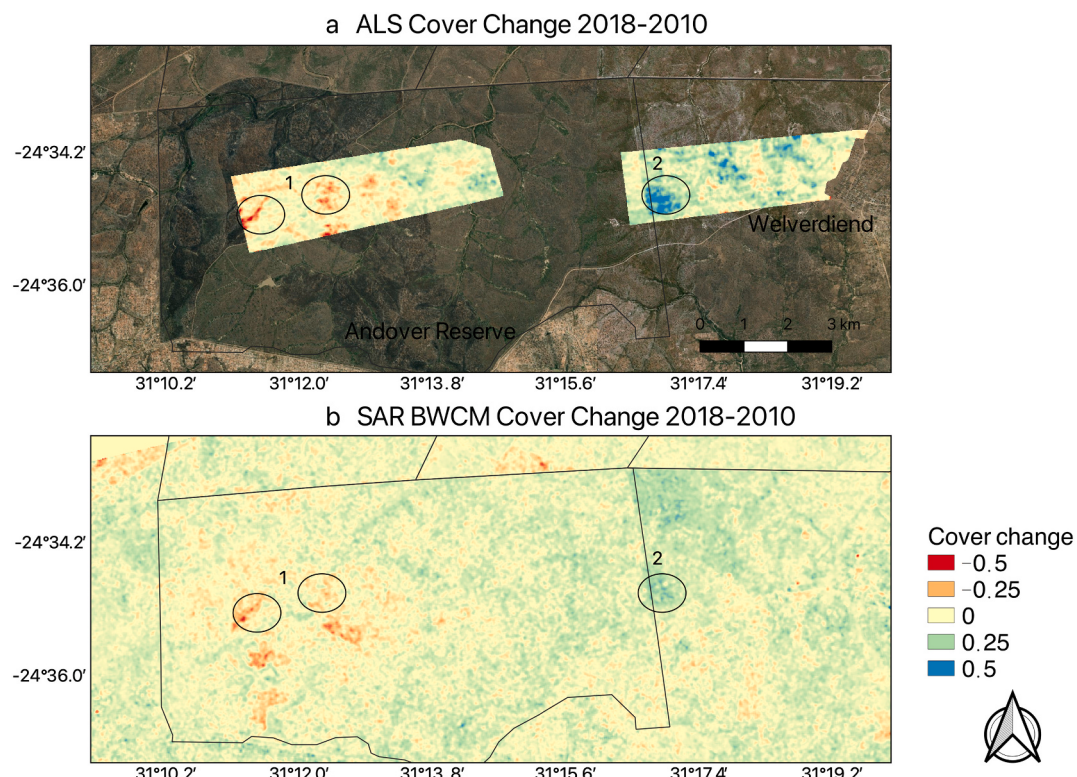


Fig. 12. Cover change between 2010 and 2018 in Andover nature reserve and neighboring communal areas (village of Welverdiend) derived from (a) ALS data aggregated to 15 m × 15 m cover change and (b) SAR-based predicted cover change using BWCM. Site 1 within Andover Reserve experienced significant large tree felling after its conservation status was challenged by neighboring communities which accessed the reserve. Site 2 experienced shrub thickening or coppice regrowth in communal areas.

approach had a slightly lower R^2 , a slightly better RMSE and most importantly, was less biased than the product difference approaches (BWCM and Log models).

The SAR-derived cover change maps, for example the BWCM product difference maps, successfully detected the loss of stands of big trees due to illegal logging in the communal rangelands and Andover Reserve, as well as elephant and fire impacts in Sabi Sands Nature Reserve (Figs. 11 and 12) (Asner et al., 2016; de Boer et al., 2015; Mograbi et al., 2017; Shannon et al., 2008, 2011). Further, the loss of big trees (> 5 m high) was extracted from the 1 m ALS CHM change data and compared with the SAR-derived cover change maps (specifically BWCM) (Fig. 14, site 1). It is apparent that localized loss of clumps of >10–20 trees resulted in a reduction in cover of up to 0.4 detected by the BWCM change product, while it was not the case for the loss of dispersed individual large trees. Note that these patterns were not consistent throughout all the study sites. Furthermore, the loss of big trees can be interspersed with shrub increases (Fig. 15, site 2), resulting in a positive cover change detected by the SAR at the 15 m–75 m level. This highlights the highly heterogeneous structure and temporal dynamics of savanna vegetation and the challenges involved in quantifying contrasting, but collocated changes, in this case the loss of big trees and gain of shrubs. The inability to distinguish these different types of woody vegetation changes at different heights (i.e. tall trees >5 m vs. shrubs <3 m) is major limitation of the backscatter-based cover change approach from a management perspective. However repeat-pass interferometric SAR has the potential to estimate woody vegetation height (Lei et al., 2017; Lei and Siqueira, 2014) and this approach is currently being investigated in savannas.

Widespread increases in cover of 0.35–0.65 in communal rangelands were indicated by all the SAR-derived change maps. Closer investigation of the ALS CHM height changes at 1 m resolution confirms that landscape-wide increases in woody vegetation that were typically <3 m in year 1 (e.g. 2010) and grew >2 m in height by year 2 (e.g. 2018), but

still remained <5 m, were responsible for the vast majority of cover increases (Fig. 14, area 1). This can be attributed to widely published shrub encroachment in the savannas of southern Africa (Buitewerf et al., 2012; O'Connor et al., 2014; Skowno et al., 2017; Stevens et al., 2017; Venter et al., 2018). In communal areas, shrub cover increases can also be caused by compensatory regrowth of coppiced woody vegetation following fuelwood harvesting, as previously described (Twine and Holdo, 2016) and quantified in this study area using ALS data (Mograbi et al., 2015). Mograbi et al., 2015 uncovered very rapid regrowth of coppiced vegetation <3 m following wood harvesting around villages in communal areas where there is a heavy dependence on fuelwood as the primary household energy source (Madubansi and Shackleton, 2007; Matsika et al., 2013; Wessels et al., 2013). The results of the current study confirm that L-band SAR backscatter is sensitive to long-term increases in woody vegetation cover and volume due to short stature shrub growth (Wessels et al., 2019), even though the specific height of the cover change cannot be derived from the backscatter alone.

In contrast to widespread woody cover increases in communal rangelands, the SAR-derived maps suggest that cover generally decreased in adjacent conservation areas, forming distinct fence-line contrast along the boundaries of the reserves that have fortified fences that restrict the movements of animals, especially elephants (Fig. 13, site 3). Although the nature of these cover decreases cannot be exactly characterized outside of the extents of the ALS data areas, studies in the neighboring and connected (not separated by fences) Kruger National Park have documented the impacts of the doubling of elephant numbers during the past 20+ years (Asner et al., 2016; Asner and Levick, 2012) and fire management practices (Eckhardt et al., 2000; Smit et al., 2010, 2016; Van Wilgen et al., 2004). The study therefore demonstrated that L-band SAR could be used for regional monitoring of gradual increases and decreases in woody vegetation cover and is the first study to our knowledge to demonstrate this using repeat ALS data in savannas.

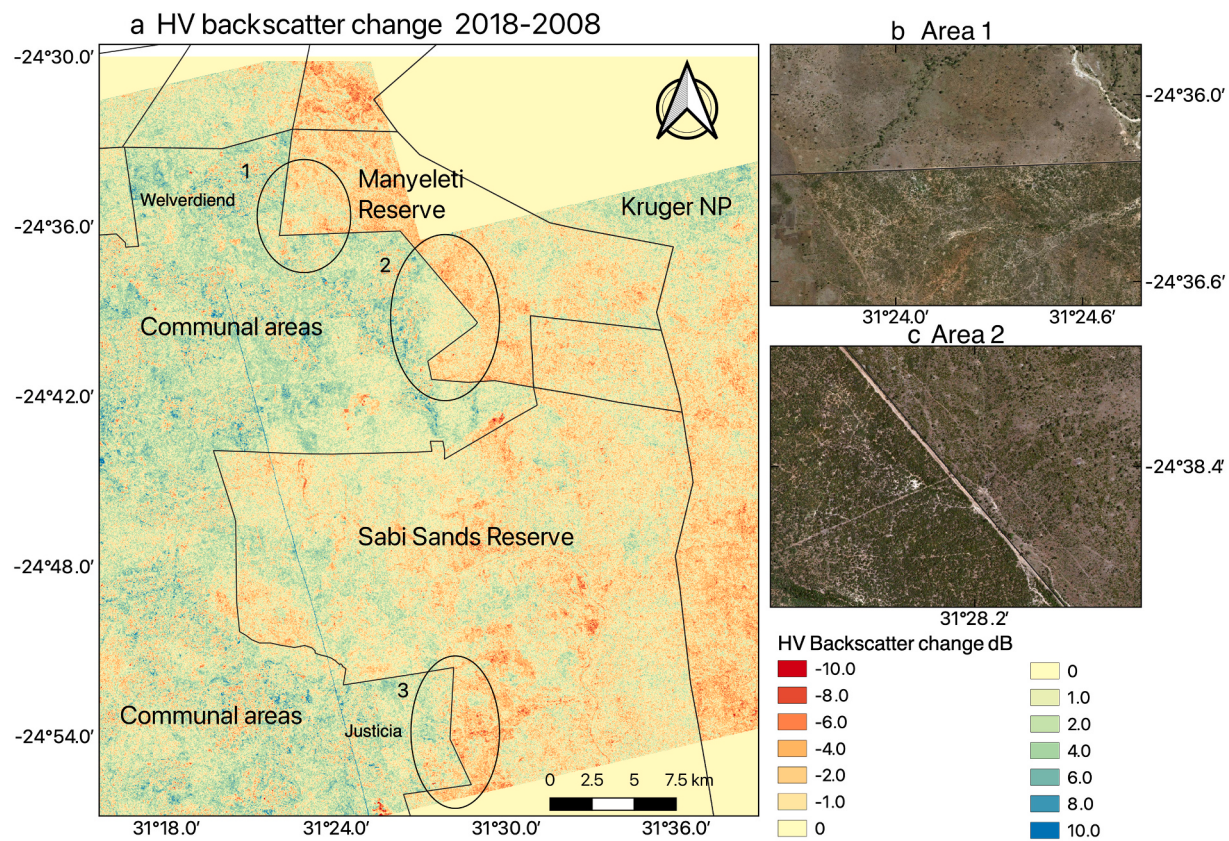


Fig. 13. (a) Regional mosaic of backscatter change (HV, 15 m × 15 m), 2018–2008. Significant reductions in $\Delta\gamma^0$ associated with woody cover decreases are most likely caused by the impact of high elephant numbers and prescribed burns within conservation areas, Manyeleti Reserve (sites 1, 2) and Sabi Sands Reserve (site 3). Increases in cover in communal areas could be due to shrub encroachment in absence of elephants and frequent wildfires. Black lines are reserve boundaries. (b and c) Recent high resolution optical image showing lower woody cover inside the Manyeleti Reserve compared to communal areas outside. (Image: Google, © 2020 Maxar Technologies)

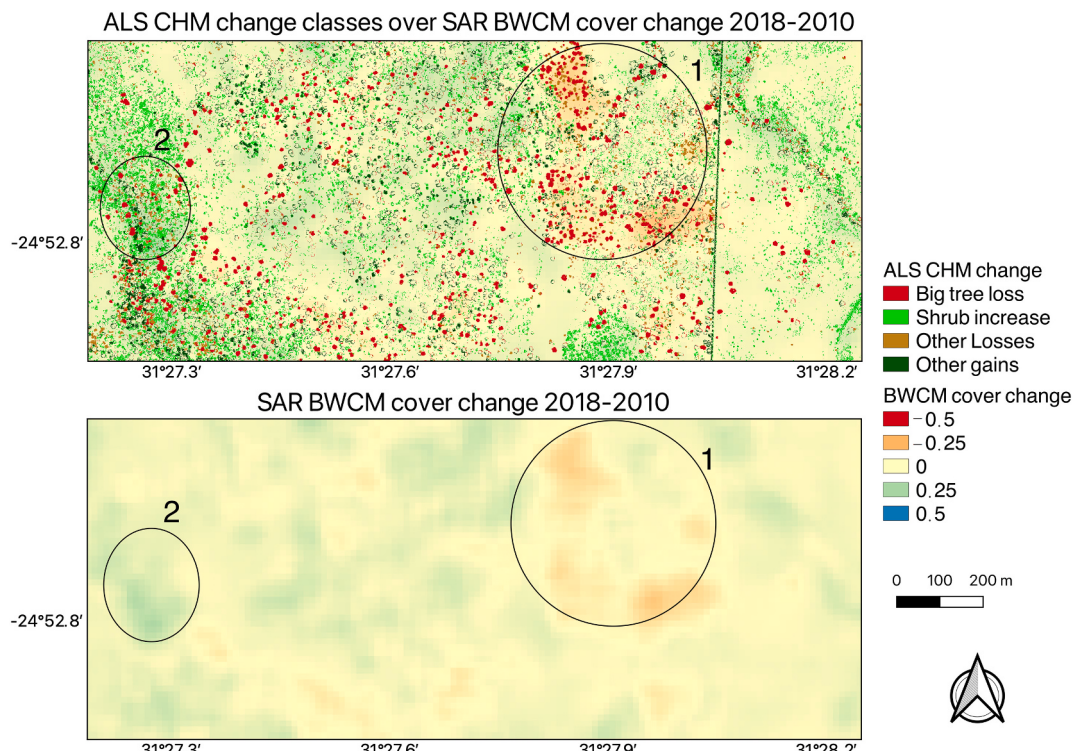


Fig. 14. Zoom-in of Airborne LiDAR (ALS CHM) vegetation change classes (1 m GSD) displayed over BWCM predicted cover changes (15 m GSD) for an area on the boundary between a communal rangeland (east of village of Justicia) and Sabi Sands Reserve (Fig. 13, site 3). (bottom) BWCM predicted cover changes without ALS overlay for same area as top.

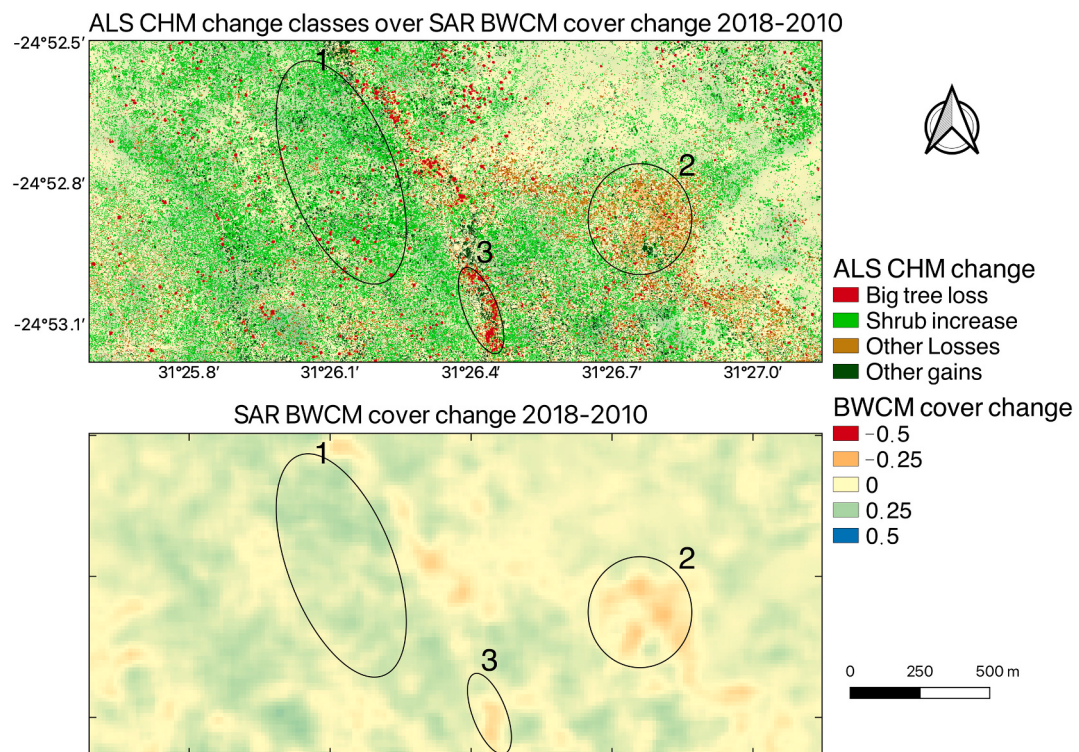


Fig. 15. (top) Zoom-in of Airborne LiDAR (ALS CHM) vegetation change classes (1 m GSD) displayed over BWCM predicted cover changes (15 m GSD) in a communal rangeland near settlement of Justicia. (bottom) BWCM predicted cover changes without ALS overlay for same area as top.

7. Conclusions

The study made use of rare repeat ALS datasets to provide novel insights into the sensitivity of L-band SAR to quantify short (2 year) and longer-term (8–10 year) changes in low biomass savannas. The results demonstrated a strong linear relationship between cover changes and backscatter change ($HV \Delta\gamma^0$) with R^2 of 0.4–0.7 and RMSE of 0.09–0.15. The results suggest that $HV \Delta\gamma^0$ can be used to directly map discernable cover change classes at 0.25 increments. It is estimated that backscatter increased or decreased about 1 dB when fractional cover increased or decreased by 0.1. This exceeds expectations of L-band SAR sensitivity to vegetation structure change, as well as the NISAR mission requirements of detecting >50% cover change (NISAR, 2018). The direct backscatter change model and the two cover product change models (BWCM and Log) had very similar uncertainties when predicting cover change with mean RMSE = 0.15, which is 13% of the observed cover change range (−0.6 to +0.6). However, the direct backscatter change approach had less underestimation of positive and negative cover change, which was above 50% bias for most of the year-pairs, across the range of Δ_{ALS} (Fig. 10). This consistent underestimation of change by the SAR-based models is one of the greatest weaknesses of this overall approach.

The SAR predicted cover change maps corresponded closely with the ALS derived change maps and captured regional patterns of change that are believed to indicate different management impacts, for example: fence-line contrasts between (i) conservation areas with cover losses due to the impacts of fire and large herbivores (Asner and Levick, 2012; Smit et al., 2010), and (ii) neighboring communal rangelands that show cover gains due to widespread shrub encroachment and compensatory coppice regrowth after fuelwood harvesting (Mograbi et al., 2019). The study therefore demonstrated that L-band SAR could be used for regional monitoring of gradual increases and decreases in savanna woody vegetation cover. This is a topic of ongoing research which is being expanded to global savannas. The findings bode well for the imminent NISAR mission as it demonstrates L-band sensitivity to low biomass and low stature regrowth which illustrates the intended expansion of the sensor's

utility to a broad diversity of ecosystems, including Tropical Dry Forests and Shrublands (FAO, 2015). In addition, NISAR's frequent 12-day repeat pass acquisitions will help reduce the impacts of environmental noise (e.g. surface moisture) and enable repeat-pass InSAR techniques to improve woody vegetation characterization, disturbance detection (Lei et al., 2019; Lei and Siqueira, 2014) and more accurate biomass estimates (Marshak et al., 2020; NISAR, 2018).

Author's responsibilities

KW conceptualized the research, secured ALS data acquisition, analyzed the data and wrote the paper. XL processed the ALS data and SAR products, analyzed data and wrote the paper. AB acquired and processed SAR data, provided technical oversight and wrote the paper. R Mathieu conceptualized the research, secured ALS data acquisition and wrote the paper. R Main and LN processed the ALS data, provided study area expertise and edited the paper. BE secured ALS data acquisition, provided expertise on savanna ecology and edited the paper. GA initiated the 2008, 2010 ALS data acquisitions and edited the paper.

Funding

The ALOS PALSAR and ALOS-2 PALSAR-2 data used in this study is owned by JAXA, Japan and was provided through an EO-RA2 Collaborative Research Agreement (PI No. ER2A2N104). The data collected by the Global Airborne Observatory (formerly Carnegie Airborne Observatory) was funded by the Mellon Foundation. The Global Airborne Observatory is made possible by support provided by private foundations, visionary individuals, and Arizona State University. This research was partially funded by NASA Carbon Monitoring System award 80NSSC21K0967 and the CSIR Strategic Research Panel.

Declaration of Competing Interest

The authors declare that they have no known competing financial

interests or personal relationships that could have appeared to influence the work reported in this paper.

Data availability

The authors do not have permission to share data.

Appendix A. Supplementary data

Supplementary data to this article can be found online at <https://doi.org/10.1016/j.rse.2022.113369>.

References

- Anchang, J.Y., Prihodko, L., Ji, W., Kumar, S.S., Ross, C.W., Yu, Q., Lind, B., Sarr, M.A., Diouf, A.A., Hanan, N.P., 2020. Toward operational mapping of Woody canopy cover in tropical savannas using Google Earth Engine. *Front. Environ. Sci.* 8 <https://doi.org/10.3389/fenvs.2020.00004>.
- ArcGIS Pro, 2021. Version 2.7. Redlands, California (2.7) Environmental Systems Research Institute (2020).
- Asner, G.P., 2007. Carnegie airborne observatory: in-flight fusion of hyperspectral imaging and waveform light detection and ranging for three-dimensional studies of ecosystems. *J. Appl. Remote. Sens.* 1, 013536 <https://doi.org/10.1117/1.2794018>.
- Asner, G.P., Levick, S.R., 2012. Landscape-scale effects of herbivores on treefall in African savannas. *Ecol. Lett.* 15, 1211–1217.
- Asner, G.P., Levick, S.R., Kennedy-Bowdoin, T., Knapp, D.E., Emerson, R., Jacobson, J., Colgan, M.S., Martin, R.E., 2009. Large-scale impacts of herbivores on the structural diversity of African savannas. In: *Proceedings of the National Academy of Sciences, USA* 106, pp. 4947–4952.
- Asner, G.P., Vaughn, N., Smit, I.P.J., Levick, S., 2016. Ecosystem-scale effects of megafauna in African savannas. *Ecography* 39, 240–252. <https://doi.org/10.1111/ecog.01640>.
- Bastin, J.-F., Berrahmouni, N., Grainger, A., Maniatis, D., Mollicone, D., Moore, R., Patriarca, C., Picard, N., Sparrow, B., Abraham, E.M., Aloui, K., Atesoglu, A., Attore, F., Bassiliū, C., Bey, A., Garzuglia, M., García-Montero, L.G., Groot, N., Guerin, G., Laestadius, L., Lowe, A.J., Mamane, B., Marchi, G., Patterson, P., Rezende, M., Ricci, S., Salcedo, I., Diaz, A.S.-P., Stolle, F., Surappaeva, V., Castro, R., 2017. The extent of forest in dryland biomes. *Science* 356, 635–638. <https://doi.org/10.1126/science.aam6527>.
- Bergen, K.M., Dobson, M.C., 1999. Integration of remotely sensed radar imagery in modeling and mapping of forest biomass and net primary production. *Ecol. Model.* 122, 257–274.
- Bergen, K.M., Goetz, S.J., Dubayah, R.O., Henebry, G.M., Hunsaker, C.T., Imhoff, M.L., Nelson, R.F., Parker, G.G., Radeloff, V.C., 2009. Remote sensing of vegetation 3-D structure for biodiversity and habitat: Review and implications for lidar and radar spaceborne missions. *Journal of Geophysical Research: Biogeosciences* 114.
- da Bispo, P.C., Rodriguez-Veiga, P., Zimbres, B., de Miranda, S.C., Giusti Cezare, C.H., Fleming, S., Baldacchino, F., Louis, V., Rains, D., Garcia, M., Espírito-Santo, F.D.B., Roitman, I., Pacheco-Pascagaza, A.M., Gou, Y., Roberts, J., Barrett, K., Ferreira, L.G., Shimbo, J.Z., Alencar, A., Bustamante, M., Woodhouse, I.H., Sano, E.E., Ometto, J.P., Tansey, K., Balzter, H., 2020. Woody aboveground biomass mapping of the Brazilian savanna with a multi-sensor and machine learning approach. *Remote Sens.* 12, 2685. <https://doi.org/10.3390/rs12172685>.
- Bond, W.J., 2008. What limits trees in C4 grasslands and savannas? *Annu. Rev. Ecol. Evol. Syst.* 39, 641–659. <https://doi.org/10.1146/annurev.ecolsys.39.110707.173411>.
- Bond, W.J., Midgley, G.F., 2012. Carbon dioxide and the uneasy interactions of trees and savanna grasses. *Philos. Trans. R. Soc. B-Biol. Sci.* 367, 601–612. <https://doi.org/10.1098/rstb.2011.0182>.
- Bouvet, A., Mermoz, S., Le Toan, T., Villard, L., Mathieu, R., Naidoo, L., Asner, G.P., 2018. An above-ground biomass map of African savannahs and woodlands at 25m resolution derived from ALOS PALSAR. *Remote Sens. Environ.* 206, 156–173.
- Brock, N.V.L., Lent, R.A., 1999. Vertical structure. In: Hunter, I., Malcom, L. (Eds.), *Maintaining Biodiversity in Forest Ecosystem*. Cambridge University Press, Cambridge, pp. 373–399.
- Bruniquel, J., Lopes, A., 1997. Multi-variate optimal speckle reduction in SAR imagery. *Int. J. Remote Sens.* 18, 603–627.
- Buitenhof, R., Bond, W.J., Stevens, N., Trollope, W.S.W., 2012. Increased tree densities in South African savannas: >50 years of data suggests CO₂ as a driver. *Glob. Chang. Biol.* 18, 675–684. <https://doi.org/10.1111/j.1365-2486.2011.02561.x>.
- Camarretta, N., Harrison, P.A., Bailey, T., Potts, B., Lucieer, A., Davidson, N., Hunt, M., 2019. Monitoring forest structure to guide adaptive management of forest restoration: a review of remote sensing approaches. *New For.* <https://doi.org/10.1007/s11056-019-09754-5>.
- Carreiras, J.M.B., Melo, J.B., Vasconcelos, M.J., 2013. Estimating the above-ground biomass in Miombo savanna woodlands (Mozambique, East Africa) using L-band synthetic aperture radar data. *Remote Sens.* 5, 1524–1548. <https://doi.org/10.3390/rs5041524>.
- Cartus, O., Kellndorfer, J., Walker, W., Franco, C., Bishop, J., Santos, L., Fuentes, J., 2014. A national, detailed map of forest aboveground carbon stocks in Mexico. *Remote Sens.* 6, 5559–5588. <https://doi.org/10.3390/rs6065559>.
- Cartus, O., Siqueira, P., Kellndorfer, J., 2018. An error model for mapping forest cover and forest cover change using L-band SAR. *IEEE Geosci. Remote Sens. Lett.* 15, 107–111. <https://doi.org/10.1109/LGRS.2017.2775659>.
- Chidumayo, E.N., Gumbo, D.J., 2010. The dry forests and woodlands of Africa: managing for products and services. *Earthscan*.
- Clark, M.L., Roberts, D.A., Ewel, J.J., Clark, D.B., 2011. Estimation of tropical rain forest aboveground biomass with small-footprint lidar and hyperspectral sensors. *Remote Sens. Environ.* 115, 2931–2942. <https://doi.org/10.1016/j.rse.2010.08.029>.
- CloudCompare, 2019. CloudCompare (version 2.10)[GPL Software].
- Coetzer-Hanack, K.L., Witkowski, E.T.F., Erasmus, B.F., 2016. Thresholds of change in a multi-use conservation landscape of South Africa: historical land-cover, future transformation and consequences for environmental decision-making. *Environ. Conserv.* 43, 253–262.
- Colgan, M.S., Asner, G.P., Levick, S.R., Martin, R.E., Chadwick, O.A., 2012. Topo-edaphic controls over woody plant biomass in South African savannas. *Biogeosci. Discuss.* 9, 957–987. <https://doi.org/10.5194/bgd-9-957-2012>.
- Colgan, M.S., Asner, G.P., Swemmer, T., 2013. Harvesting tree biomass at the stand level to assess the accuracy of field and airborne biomass estimation in savannas. *Ecol. Appl.* 23, 1170–1184.
- Davies, A.B., Gaylard, A., Asner, G.P., 2018. Megafaunal effects on vegetation structure throughout a densely wooded African landscape. *Ecol. Appl.* 28, 398–408. <https://doi.org/10.1002/eaap.1655>.
- de Boer, W.F., Van Oort, J.W., Grover, M., Peel, M.J., 2015. Elephant-mediated habitat modifications and changes in herbivore species assemblages in Sabi Sand, South Africa. *Eur. J. Wildl. Res.* 61, 491–503.
- De Grandi, G.D., Bouvet, A., Lucas, R.M., Shimada, M., Monaco, S., Rosenqvist, A., 2011. The K&C PALSAR mosaic of the African continent: processing issues and first thematic results. *IEEE Trans. Geosci. Remote Sens.* 49, 3593–3610.
- Dean, W.R.J., Milton, S.J., Jettsch, F., 1999. Large trees, fertile islands, and birds in arid savanna. *J. Arid Environ.* 41, 61–78. <https://doi.org/10.1006/jare.1998.0455>.
- Dobson, M.C., Ulaby, F.T., Le Toan, T., Beaudion, A., Kaschischke, E.S., Christensen, N., 1992. Dependence of radar backscatter on coniferous forest biomass. *IEEE Trans. Geosci. Remote Sens.* 30, 412–415.
- Eckhardt, H.C., Van Wilgen, B.W., Biggs, H.C., 2000. Trends in woody vegetation cover in the Kruger National Park, South Africa, between 1940 and 1998. *Afr. J. Ecol.* 38, 108–115.
- FAO, 2020. The State of the World's Forests 2020, The State of the World's Forests 2020. FAO and UNEP. <https://doi.org/10.4060/ca8642en>.
- FAO, 2015. Global ecological zones for FAO forest reporting: 2010 Update. FAO, Rome, Italy.
- Farr, T.G., Kobrick, M., 2000. Shuttle Radar Topography Mission produces a wealth of data. *Eos, Trans. Am. Geophys. Union* 81, 583–585.
- Fisher, J., Witkowski, E.T.F., Erasmus, B.F.N., van Aardt, J.A.N., Asner, G.P., Wessels, K.J., Mathieu, R., 2012. Human-modified landscapes: patterns of fine-scale woody vegetation structure in communal savanna rangelands. *Environ. Conserv.* 39, 72–82.
- Fisher, J.T., Witkowski, E.T., Erasmus, B.F., Mograbi, P.J., Asner, G.P., Aardt, J.A., Wessels, K.J., Mathieu, R., 2015. What lies beneath: detecting sub-canopy changes in savanna woodlands using a three-dimensional classification method. *Appl. Veg. Sci.* 18, 528–540.
- Fuller, W.A., 2009. *Measurement Error Models*. John Wiley & Sons, New York, NY, USA.
- Grace, J., Jose, J.S., Meir, P., Miranda, H.S., Montes, R.A., 2006. Productivity and carbon fluxes of tropical savannas. *J. Biogeogr.* 33, 387–400. <https://doi.org/10.1111/j.1365-2699.2005.01448.x>.
- Hansen, M.C., Potapov, P.V., Moore, R., Hancher, M., Turubanova, S.A., Tyukavina, A., Thau, D., Stehman, S.V., Goetz, S.J., Loveland, T.R., Kommareddy, A., Egorov, A., Chini, L., Justice, C.O., Townshend, J.R., 2013. High-resolution global maps of 21st-century forest cover change. *Science* 342, 850–853. <https://doi.org/10.1126/science.1244693>.
- Hensley, S., Oveisgharan, S., Saatchi, S., Simard, M., Ahmed, R., Haddad, Z., 2013. An error model for biomass estimates derived from polarimetric radar backscatter. *IEEE Trans. Geosci. Remote Sens.* 52, 4065–4082.
- Huuya, I., Persson, H.J., Soja, M.J., Wallerman, J., Ulander, L.M.H., Fransson, J.E.S., 2020. Predictions of biomass change in a Hemi-Boreal forest based on multi-polarization L and P-band SAR backscatter. *Can. J. Remote. Sens.* 46, 661–680. <https://doi.org/10.1080/07038992.2020.1838891>.
- Jennings, S., Brown, N., Sheila, D., 1999. Assessing forest canopies and understorey illumination: canopy closure, canopy cover and other measures. *Forestry* 72, 59–73.
- Joshi, N., Mitchard, E.T., Brolly, M., Schumacher, J., Fernández-Landa, A., Johannsen, V.K., Marchamalo, M., Fensholt, R., 2017. Understanding ‘saturation’ of radar signals over forests. *Sci. Rep.* 7, 1–11.
- Joubert, D.F., Smit, G.N., Hoffman, M.T., 2013. The influence of rainfall, competition and predation on seed production, germination and establishment of an encroaching *Acacia* in an arid Namibian savanna. *J. Arid Environ.* 91, 7–13.
- Le Toan, T., Quegan, S., Woodward, I., Lomas, M., Delbart, N., Picard, G., 2004. Relating radar remote sensing of biomass to modelling of forest carbon budgets. *Clim. Chang.* 67, 379–402. <https://doi.org/10.1007/s10584-004-3155-5>.
- Lei, Y., Lucas, R., Siqueira, P., Schmidt, M., Treuhaft, R., 2017. Detection of forest disturbance with spaceborne repeat-pass SAR interferometry. *IEEE Trans. Geosci. Remote Sens.* 56, 2424–2439.
- Lei, Y., Siqueira, P., 2014. Estimation of forest height using spaceborne repeat-pass L-band InSAR correlation magnitude over the US state of Maine. *Remote Sens.* 6, 10252–10285.
- Lei, Y., Siqueira, P., Torbick, N., Ducey, M., Chowdhury, D., Salas, W., 2019. Generation of large-scale moderate-resolution forest height mosaic with spaceborne repeat-pass SAR interferometry and lidar. *IEEE Trans. Geosci. Remote Sens.* 57, 770–787. <https://doi.org/10.1109/TGRS.2018.2860590>.

- Levick, S.R., Asner, G.P., Kennedy-Bowdoin, T., Knapp, D.E., 2009. The relative influence of fire and herbivory on savanna three-dimensional vegetation structure. *Biol. Conserv.* 142, 1693–1700.
- Lucas, R.M., Cronin, N., Lee, A., Moghaddam, M., Witte, C., Tickle, P., 2006. Empirical relationships between AIRSAR backscatter and LiDAR-derived forest biomass, Queensland, Australia. *Remote Sens. Environ.* 100, 407–425. <https://doi.org/10.1016/j.rse.2005.10.019>.
- Madubansi, M., Shackleton, C.M., 2007. Changes in fuelwood use and selection following electrification in the Bushbuckridge lowveld, South Africa. *J. Environ. Manag.* 83, 416–426.
- Main, R., Mathieu, R., Kleynhans, W., Wessels, K., Naidoo, L., Asner, G., 2016. Hyper-temporal C-band SAR for baseline woody structural assessments in deciduous savannas. *Remote Sens.* 8, 661.
- Marshak, C., Simard, M., Duncanson, L., Silva, C.A., Denbina, M., Liao, T.-H., Fatoyinbo, L., Moussavou, G., Armston, J., 2020. Regional tropical aboveground biomass mapping with L-band repeat-pass interferometric radar, sparse lidar, and multiscale superpixels. *Remote Sens.* 12, 2048. <https://doi.org/10.3390/rs12122048>.
- Mathieu, R., Naidoo, L., Cho, M.A., Leblon, B., Main, R., Wessels, K., Asner, G.P., Buckley, J., Van Aardt, J., Erasmus, B.F., Smit, I.P.J., 2013. Toward structural assessment of semi-arid African savannahs and woodlands: the potential of multitemporal polarimetric RADARSAT-2 fine beam images. *Remote Sens. Environ.* 138, 215–231.
- Matsika, R., Erasmus, B.F.N., Twine, W., 2013. A tale of two villages: assessing the dynamics of fuelwood supply in communal landscapes within the Kruger to Canyons Biosphere in South Africa. *Environ. Conserv.* 40, 71–83.
- McNicol, I.M., Ryan, C.M., Mitchard, E.T.A., 2018. Carbon losses from deforestation and widespread degradation offset by extensive growth in African woodlands. *Nat. Commun.* 9, 3045. <https://doi.org/10.1038/s41467-018-05386-z>.
- Mermoz, S., Le Toan, T., 2016. Forest disturbances and regrowth assessment using ALOS PALSAR data from 2007 to 2010 in Vietnam, Cambodia and Lao PDR. *Remote Sens.* 8, 217.
- Mermoz, S., Le Toan, T., Villard, L., Réjou-Méchain, M., Seifert-Granzin, J., 2014. Biomass assessment in the Cameroonian savanna using ALOS PALSAR data. *Remote Sens. Environ.* 155, 109–119. <https://doi.org/10.1016/j.rse.2014.01.029>.
- Mitchard, E.T.A., 2009. Using satellite radar backscatter to predict above-ground woody biomass: a consistent relationship across four different African landscapes. *Geophys. Res. Lett.* 36.
- Mitchard, E.T.A., Meir, P., Ryan, C.M., Woollen, E.S., Williams, M., Goodman, L.E., Mucavele, J.A., Watts, P., Woodhouse, I.H., Saatchi, S.S., 2013. A novel application of satellite radar data: measuring carbon sequestration and detecting degradation in a community forestry project in Mozambique. *Plant Ecol. Divers.* 6, 159–170. <https://doi.org/10.1080/17550874.2012.695814>.
- Mitchard, E.T.A., Saatchi, S.S., Lewis, S.L., Feldpausch, T.R., Woodhouse, I.H., Sonke, B., Rowland, C., Meir, P., 2011. Measuring biomass changes due to woody encroachment and deforestation/degradation in a forest-savanna boundary region of central Africa using multi-temporal L-band radar backscatter. *Remote Sens. Environ.* 115, 2861–2873. <https://doi.org/10.1016/j.rse.2010.02.022>.
- Mitchell, A.L., Rosenqvist, A., Mora, B., 2017. Current remote sensing approaches to monitoring forest degradation in support of countries measurement, reporting and verification (MRV) systems for REDD+. *Carbon Balance Manag.* 12, 1–22.
- Mograbi, P.J., Asner, G.P., Witkowski, E.T.F., Erasmus, B.F.N., Wessels, K.J., Mathieu, R., Vaughn, N.R., 2017. Humans and elephants as treefall drivers in African savannas. *Ecography* 40, 1274–1284. <https://doi.org/10.1111/ecog.02549>.
- Mograbi, P.J., Erasmus, B.F.N., Witkowski, E.T.F., Asner, G.P., Wessels, K.J., Mathieu, R., Knapp, D.E., Martin, R.E., Main, R., 2015. Biomass increases Go under cover: Woody vegetation dynamics in South African rangelands. *PLoS ONE* 10, e0127093. <https://doi.org/10.1371/journal.pone.0127093>.
- Mograbi, P.J., Witkowski, E.T., Erasmus, B.F., Asner, G.P., Fisher, J.T., Mathieu, R., Wessels, K.J., 2019. Fuelwood extraction intensity drives compensatory regrowth in African savanna communal lands. *Land Degrad. Dev.* 30, 190–201.
- Mucina, L., Rutherford, M.C., 2006. The Vegetation of South Africa, Lesotho and Swaziland. Strelitzia, Cape Town.
- Naidoo, L., Mathieu, R., Main, R., Kleynhans, W., Wessels, K., Asner, G., Leblon, B., 2015. Savannah woody structure modelling and mapping using multi-frequency (X-, C- and L-band) Synthetic Aperture Radar data. *ISPRS J. Photogramm. Remote Sens.* 105, 234–250.
- Naidoo, L., Mathieu, R., Main, R., Wessels, K., Asner, G.P., 2016. L-band Synthetic Aperture Radar imagery performs better than optical datasets at retrieving woody fractional cover in deciduous, dry savannahs. *Int. J. Appl. Earth Obs. Geoinf.* 52, 54–64.
- NISAR, 2018. NASA-ISRO SAR (NISAR) Mission Science Users' Handbook. NASA Jet Propulsion Laboratory.
- O'Connor, T.G., Puttick, J.R., Hoffman, M.T., 2014. Bush encroachment in southern Africa: Changes and causes. *African J. Range Forage Sci.* 31, 67–88.
- Odipo, V.O., Nickless, A., Berger, C., Baade, J., Urbazaev, M., Walther, C., Schmullius, C., 2016. Assessment of aboveground Woody biomass dynamics using terrestrial laser scanner and L-band ALOS PALSAR data in South African Savanna. *Forests* 7. <https://doi.org/10.3390/f7120294>.
- Pollard, S., Shackleton, C.M., Currrthers, J., 2003. Beyond the fences: people and the Lowveld landscape. In: Du Toit, J., Biggs, H., Rogers, K.H. (Eds.), *The Kruger Experience: Ecology and Management of Savanna Heterogeneity*. Island Press, London, pp. 422–446.
- Quegan, S., Yu, J.J., 2001. Filtering of multichannel SAR images. *IEEE Trans. Geosci. Remote Sens.* 39, 2373–2379.
- Lucas, R., Armston, J., Fairfax, R., Fensham, R., Accad, A., Carreiras, J., Kelley, J., Bunting, P., Clewley, D., Bray, S., Metcalfe, D., Dwyer, J., Bowen, M., Eyre, T., Laidlaw, M., Shimada, M., 2010. An evaluation of the ALOS PALSAR L-band backscatter - above ground biomass relationship Queensland, Australia: impacts of surface moisture condition and vegetation structure. *IEEE J. Select. Top. Appl. Earth Observ. Remote Sens.* 3, 576–593. <https://doi.org/10.1109/jstars.2010.2086436>.
- Ratnam, J., Tomlinson, K.W., Rasquinha, D.N., Sankaran, M., 2016. Savannahs of Asia: antiquity, biogeography, and an uncertain future. *Philos. Trans. Roy. Soc. B: Biol. Sci.* 371, 20150305. <https://doi.org/10.1098/rstb.2015.0305>.
- Rejou-Mechain, M., Muller-Landau, H.C., Detto, M., Thomas, S.C., Toan, T.L., Saatchi, S.S., Barreto-Silva, J.S., Bourg, N.A., Bunyavejchewin, S., Butt, N., 2014. Local spatial structure of forest biomass and its consequences for remote sensing of carbon stocks. *Biogeosci. Discuss.* 11, 5711.
- Rignot, E.J., Van Zyl, J.J., 1993. Change detection techniques for ERS-1 SAR data. *IEEE Trans. Geosci. Remote Sens.* 31, 896–906.
- Rodríguez-Veiga, P., Quegan, S., Carreiras, J., Persson, H.J., Fransson, J.E., Hosculo, A., Ziolkowski, D., Stereńczak, K., Lohberger, S., Stångel, M., 2019. Forest biomass retrieval approaches from earth observation in different biomes. *Int. J. Appl. Earth Obs. Geoinf.* 77, 53–68.
- Rosenqvist, Å., Milne, A., Lucas, R., Imhoff, M., Dobson, C., 2003. A review of remote sensing technology in support of the Kyoto Protocol. *Environ. Sci. Policy* 6, 441–455. [https://doi.org/10.1016/S1462-9011\(03\)00070-4](https://doi.org/10.1016/S1462-9011(03)00070-4).
- Roussel, J.-R., Auty, D., De Boissieu, F., Meador, A.S., 2018. lidR: Airborne LiDAR data manipulation and visualization for forestry applications. *R package version 1*.
- Ryan, C.M., Hill, T., Woollen, E., Ghee, C., Mitchard, E., Cassells, G., Grace, J., Woodhouse, I.H., Williams, M., 2012. Quantifying small-scale deforestation and forest degradation in African woodlands using radar imagery. *Glob. Change Biol.* 18, 243–257. <https://doi.org/10.1111/j.1365-2486.2011.02551.x>.
- Sankaran, M., Hanan, N.P., Scholes, R.J., Ratnam, J., Augustine, D.J., Cade, B.S., Gignoux, J., Higgins, S.I., Le Roux, X., Ludwig, F., Ardo, J., Banyikwa, F., Bronn, A., Bucini, G., Taylor, K.K., Coughenour, M.B., Diouf, A., Ekaya, W., Feral, C.J., February, E.C., Frost, P.G.H., Hiernaux, P., Hrabar, H., Metzger, K.L., Prins, H.H.T., Ringrose, S., Sea, W., Tews, J., Worden, J., Zambatis, N., 2005. Determinants of woody cover in African savannas. *Nature* 438, 846–849. <https://doi.org/10.1038/nature04070>.
- Sankaran, M., Ratnam, J., Hanan, N., 2008. Woody cover in African savannas: the role of resources, fire and herbivory. *Glob. Ecol. Biogeogr.* 17, 236–245. <https://doi.org/10.1111/j.1466-8238.2007.00360.x>.
- Santoro, M., Askne, J., Smith, G., Fransson, J.E., 2002. Stem volume retrieval in boreal forests from ERS-1/2 interferometry. *Remote Sens. Environ.* 81, 19–35.
- Santoro, M., Cartus, O., 2018. Research pathways of forest above-ground biomass estimation based on SAR backscatter and interferometric SAR observations. *Remote Sens.* 10 <https://doi.org/10.3390/rs10040608>.
- Santoro, M., Pantze, A., Fransson, J.E.S., Dahlgren, J., Persson, A., 2012. Nation-wide clear-cut mapping in Sweden using ALOS PALSAR strip images. *Remote Sens.* 4, 1693–1715. <https://doi.org/10.3390/rs4061693>.
- Saugier, B., Roy, J., Mooney, H.A., 2001. Estimations of Global Terrestrial Productivity. *Terrestrial Global Productivity* 543–557. <https://doi.org/10.1016/b978-012505290-5/00024-7>.
- Scholes, R., Archer, S., 1997. Tree-grass interactions in savannas. *Annu. Rev. Ecol. Syst.* 28, 517–544.
- Scholes, R.J., Archer, S.R., 1997. Tree-grass interactions in savannas. *Annu. Rev. Ecol. Syst.* 28, 517–544.
- Scholes, R.J., Walker, B.H., 1993. *An African Savanna: Synthesis of the Nylsvley Study*. Cambridge University Press, Cambridge.
- Shackleton, C., 2002. Growth and fruit production of *Sclerocarya birrea* in the South African lowveld. *Agroforestry* 55, 175–180.
- Shannon, G., Druce, D.J., Page, B.R., Eckhardt, H.C., Grant, R., Slotow, R., 2008. The utilization of large savanna trees by elephant in southern Kruger National Park. *J. Trop. Ecol.* 24, 581.
- Shannon, G., Thaker, M., Vanak, A.T., Page, B.R., Grant, R., Slotow, R., 2011. Relative impacts of elephant and fire on large trees in a savanna ecosystem. *Ecosystems* 14, 1372–1381. <https://doi.org/10.1007/s10021-011-9485-z>.
- Shimada, M., Itoh, T., Motooka, T., Watanabe, M., Shiraishi, T., Thapa, R., Lucas, R., 2014. New global forest/non-forest maps from ALOS PALSAR data (2007–2010). *Remote Sens. Environ.* 155, 13–31.
- Skowno, A.L., Thompson, M.W., Hiestermann, J., Ripley, B., West, A.G., Bond, W.J., 2017. Woodland expansion in South African grassy biomes based on satellite observations (1990–2013): general patterns and potential drivers. *Glob. Chang. Biol.* 23, 2358–2369. <https://doi.org/10.1111/gcb.13529>.
- Smit, I.P.J., Asner, G.P., Govender, N., Kennedy-Bowdoin, T., Knapp, D.E., Jacobson, J., 2010. Effects of fire on woody vegetation structure in African savanna. *Ecol. Appl.* 20, 1865–1875.
- Smit, I.P.J., Asner, G.P., Govender, N., Vaughn, N.R., van Wilgen, B.W., 2016. An examination of the potential efficacy of high-intensity fires for reversing woody encroachment in savannas. *J. Appl. Ecol.* 53, 1623–1633. <https://doi.org/10.1111/1365-2664.12738>.
- Smit, I.P.J., Prins, H.H.T., 2015. Predicting the effects of woody encroachment on mammal communities, grazing biomass and fire frequency in African Savannas. *PLOS ONE* 10, e0137857. <https://doi.org/10.1371/journal.pone.0137857>.
- Smith, W.K., Dannenberg, M.P., Yan, D., Herrmann, S., Barnes, M.L., Barron-Gafford, G.A., Biederman, J.A., Ferrenberg, S., Fox, A.M., Hudson, A., Knowles, J.F., MacBean, N., Moore, D.J.P., Nagler, P.L., Reed, S.C., Rutherford, W.A., Scott, R.L., Wang, X., Yang, J., 2019. Remote sensing of dryland ecosystem structure and function: progress, challenges, and opportunities. *Remote Sens. Environ.* 233, 111401 <https://doi.org/10.1016/j.rse.2019.111401>.

- SNAP - ESA, 2022. Sentinel Application Platform.
- Southworth, J., Zhu, L., Bunting, E., Ryan, S.J., Herrero, H., Waylen, P.R., Hill, M.J., 2016. Changes in vegetation persistence across global savanna landscapes, 1982–2010. *J. Land Use Sci.* 11, 7–32.
- Staver, A., Archibald, S., Levin, S., 2011. Tree cover in sub-Saharan Africa: rainfall and fire constrain forest and savanna as alternative stable states. *Ecology* 92, 1063–1072.
- Stevens, N., Erasmus, B.F.N., Archibald, S., Bond, W.J., 2016. Woody encroachment over 70 years in South African savannahs: Overgrazing, global change or extinction aftershock? *Philos.Trans.Roy. Soc.B Biol.Sci.* 371 <https://doi.org/10.1098/rstb.2015.0437>.
- Stevens, N., Lehmann, C.E., Murphy, B.P., Durigan, G., 2017. Savanna woody encroachment is widespread across three continents. *Glob. Chang. Biol.* 23, 235–244.
- Thorne, M.S., Skinner, Q.D., Smith, M.A., Rodgers, J.D., Laycock, W.A., Cerekci, S.A., 2002. Evaluation of a technique for measuring canopy volume of shrubs. *J. Range Manag.* 55, 235–241. <https://doi.org/10.2307/4003129>.
- Tian, F., Brandt, M., Liu, Y.Y., Rasmussen, K., Fensholt, R., 2017. Mapping gains and losses in woody vegetation across global tropical drylands. *Glob. Chang. Biol.* 23, 1748–1760. <https://doi.org/10.1111/gcb.13464>.
- Turner, M.G., Gardner, R.H., 2001. Landscape ecology in theory and practice: pattern and process. In: *Landscape Ecology in Theory and Practice: Pattern and Process*, second edition. Springer, New York.
- Twine, W., Siphugu, V., Moshe, D., 2003. Harvesting of communal resources by “outsiders” in rural South Africa: a case of xenophobia or a real threat to sustainability? *Int. J. Sust. Dev. World* 10, 263–274.
- Twine, W.C., Holdo, R.M., 2016. Fuelwood sustainability revisited: integrating size structure and resprouting into a spatially realistic fuelshed model. *J. Appl. Ecol.* 53, 1766–1776.
- Urbazaev, M., Thiel, C., Cremer, F., Dubayah, R., Migliavacca, M., Reichstein, M., Schmullius, C., 2018. Estimation of forest aboveground biomass and uncertainties by integration of field measurements, airborne LiDAR, and SAR and optical satellite data in Mexico. *Carbon Balance Manag.* 13, 5. <https://doi.org/10.1186/s13021-018-0093-5>.
- Urbazaev, M., Thiel, C., Mathieu, R., Naidoo, L., Levick, S.R., Smit, I.P.J., Asner, G.P., Schmullius, C., 2015. Assessment of the mapping of fractional woody cover in southern African savannas using multi-temporal and polarimetric ALOS PALSAR L-band images. *Remote Sens. Environ.* 166, 138–153. <https://doi.org/10.1016/j.rse.2015.06.013>.
- Van Wilgen, B.W., Govender, N., Biggs, H.C., Ntsala, D., Funda, X.N., 2004. Response of savanna fire regimes to changing fire-management policies in a large African national park. *Conserv. Biol.* 18, 1535–1540.
- Venter, Z.S., Cramer, M.D., Hawkins, H.-J., 2018. Drivers of woody plant encroachment over Africa. *Nat. Commun.* 9, 2272. <https://doi.org/10.1038/s41467-018-04616-8>.
- Villard, L., 2009. *Forward & Inverse Modeling for Synthetic Aperture Radar Observables in Bistatic Configuration. Applications in Forest Remote Sensing*. Institut Supérieur de l’Aéronautique et de l’Espace.
- Wagenseil, H., Samimi, C., 2007. Woody vegetation cover in Namibian savannahs: a modelling approach based on remote sensing. *Erdkunde* 61, 325–334.
- Wessels, K., Mathieu, R., Knox, N., Main, R., Naidoo, L., Steenkamp, K., 2019. Mapping and monitoring fractional woody vegetation cover in the arid savannas of Namibia using LiDAR training data, machine learning, and ALOS PALSAR data. *Remote Sens.* 11, 2633.
- Wessels, K.J., Colgan, M.S., Erasmus, B.F.N., Asner, G.P., Twine, W.C., Mathieu, R., van Aardt, J.A.N., Fisher, J.T., Smit, I.P.J., 2013. Unsustainable fuelwood extraction from South African savannas. *Environ. Res. Lett.* 8, 014007 <https://doi.org/10.1088/1748-9326/8/1/014007>.
- Wessels, K.J., Mathieu, R., Erasmus, B.F.N., Asner, G.P., Smit, I.P.J., van Aardt, J.A.N., Main, R., Fisher, J., Marais, W., Kennedy-Bowdoin, T., Knapp, D.E., Emerson, R., Jacobson, J., 2011. Impact of communal land use and conservation on woody vegetation structure in the Lowveld savannas of South Africa. *For. Ecol. Manag.* 261, 19–29. <https://doi.org/10.1016/j.foreco.2010.09.012>.
- Wingate, V.R., Phinn, S.R., Kuhn, N., Scarth, P., 2018. Estimating aboveground woody biomass change in Kalahari woodland: combining field, radar, and optical data sets. *Int. J. Remote Sens.* 39, 577–606. <https://doi.org/10.1080/01431161.2017.1390271>.
- Woodhouse, I.H., 2006. Introduction to Microwave Remote Sensing. In: *Introduction to Microwave Remote Sensing*, 1st Editio. ed. CRC Press. <https://doi.org/10.1201/9781315272573>.
- Woodhouse, I.H., Mitchard, E.T.A., Brolly, M., Maniatis, D., Ryan, C.M., 2012. Radar backscatter is not a “direct measure” of forest biomass. *Nat. Clim. Chang.* 2, 556–557. <https://doi.org/10.1038/nclimate1601>.
- Yu, Y., Saatchi, S., 2016. Sensitivity of L-band SAR backscatter to aboveground biomass of global forests. *Remote Sens.* 8, 522. <https://doi.org/10.3390/rs8060522>.
- Zimbres, B., Rodriguez-Veiga, P., Shimbo, J.Z., Balzter, H., Bustamante, M., Roitman, I., Haider, R., Miranda, S., Gomes, L., Carvalho, F.A., Lenza, E., Maracahipes-Santos, L., Abadia, A.C., do Prado Junior, J.A., Mendonca Machado, E.L., Dias Gonzaga, A.P., de Mello, J.M., Soares Scolforo, J.R., Rodrigues Pinto, J.R., Alencar, A., 2021. Mapping the stock and spatial distribution of aboveground woody biomass in the native vegetation of the Brazilian Cerrado biome. *For. Ecol. Manage.* 499, 119615. <https://doi.org/10.1016/j.foreco.2021.119615>.